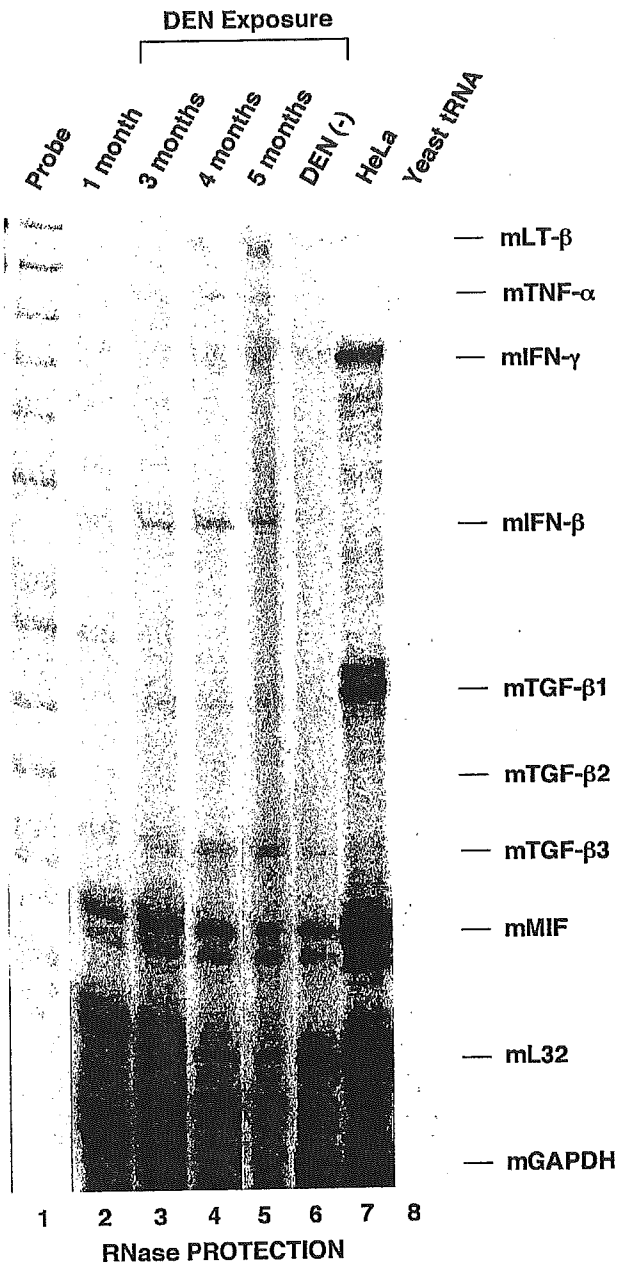

Figure 3 Analysis of intrahepatic cytokine mRNA expression in wt mice after diethylnitrosamine (DEN) exposure. Total RNA (15 μg) was extracted from nontumorous liver tissue of representative mice killed and subjected to RNase protection assay to monitor the expression of a panel of inflammatory cytokines. Intrahepatic LT-β, TNF-α, IFN-γ, IFN-β, TGF-β1, and TGF-β3 mRNA appeared after 1 month of DEN exposure and remained elevated. The housekeeping genes, ribosomal protein light 32 (L32), and glyceraldehyde-3-phosphate dehydrogenase (GAPDH) were used to normalize the amount of RNA loaded in each lane.

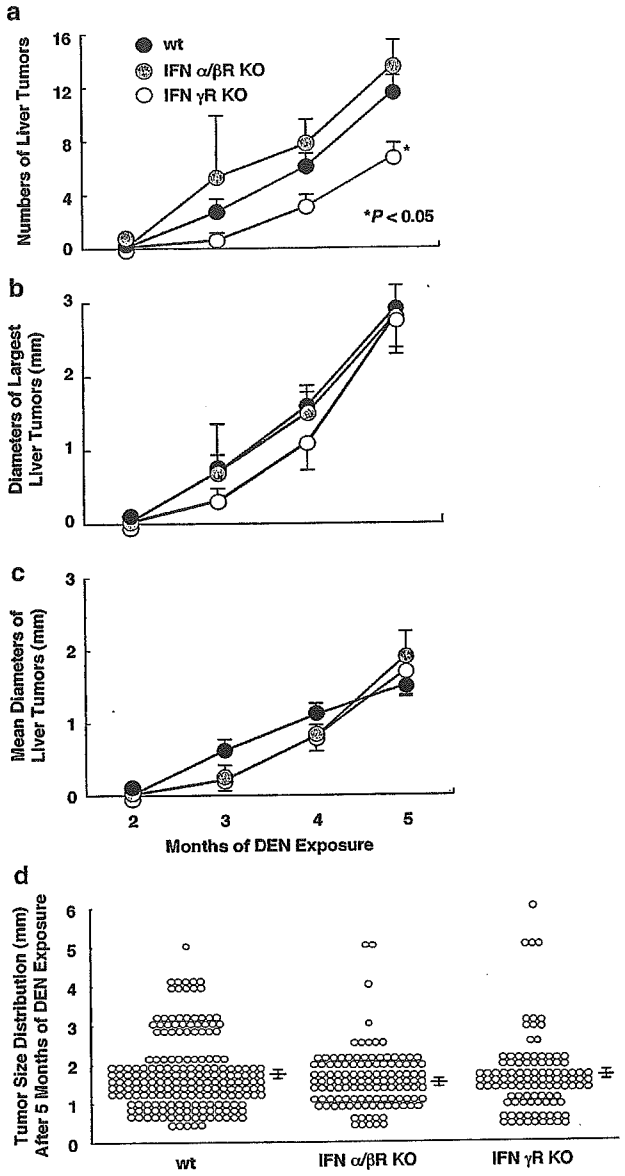

Figure 4 Tumor development in the livers of IFN-γR KO, IFN-α/βR KO, and wt mice exposed to diethylnitrosamine (DEN) in drinking water. Numbers of liver tumors, diameters of the largest liver tumors, and the mean diameters of the liver tumors were determined at autopsy. (**a**) At 5 months after DEN exposure, IFN-γR KO mice developed fewer tumors than IFN-α/βR KO and wt mice ($P<0.05$). (**b**) The diameters of the largest liver tumors were not significantly different among the three lineages. (**c**) The mean diameters of the liver tumors were not significantly different among the three lineages. (**d**) Tumor size distribution after 5 months of DEN exposure was not significantly different among the three lineages. At 2 months, $n=13$, 5, and 12 in wt, IFN-α/βR KO, and IFN-γR KO mice, respectively; 3 months, $n=13$, 3, and 10, respectively; 4 months, $n=17$, 12 and 15, respectively; 5 months, $n=17$, 9 and 16, respectively.

were comparable between IFN-γR KO and wt mice (CYP2E1 activities (±s.d.) (pmol/mg/min): 746.4±291.7 and 424.1±76.4, respectively; not significant). In addition, CYP2E1 activities of IFN-γR KO and wt mice without exposure to DEN were also comparable (CYP2E1 activities (±s.d.) (pmol/mg/min): 3005.6±286.6 and 2530.6±305.0, respectively; not significant). These data suggest that these

strains may have similar capacity to activate DEN in their liver tissues.

Inflammatory Reactions in the Livers of IFN-α/βR KO and IFN-γR KO Mice

To understand the effect of IFNs on inflammatory cell infiltration during the process of chemical hepatocarcinogenesis induced by DEN, liver samples collected from IFN-α/βR KO mice, IFN-γR KO mice, and wt mice were stained and the numbers of infiltrating mononuclear cells were counted. Numbers of infiltrating mononuclear cells were similar among three lineages (3 months; wt mice, $1597 \pm 502/mm^2$; IFN-α/βR KO mice, $640 \pm 280/mm^2$; IFN-γR KO mice, $890 \pm 122/mm^2$; not significant). Furthermore, liver section samples were stained immunohistochemically with a rat monoclonal antibody to mouse macrophages. In wt mice, the proportion of macrophages increased over the period studied (2 months, $13.3 \pm 3.3\%$; 3 months, $16.7 \pm 3.3\%$; 4 months, $20.0 \pm 0.1\%$; and 5 months, $32.5 \pm 10.3\%$). In contrast to IFN-α/βR KO and wt mice, IFN-γR KO mice had reduced proportions of macrophages in the liver (Figure 5). In addition, to evaluate the activation status of inflammatory infiltrates, intrahepatic expression of inflammatory cytokines was analyzed using an RNase protection assay. Intrahepatic expression of TNF-α, IFN-γ, and IFN-β was lower in IFN-γR KO mice than wt mice (Figure 6). Collectively, the data suggest that IFN-γ-induced activation of macrophages may be involved in the process of DEN-induced chemical hepatocar-

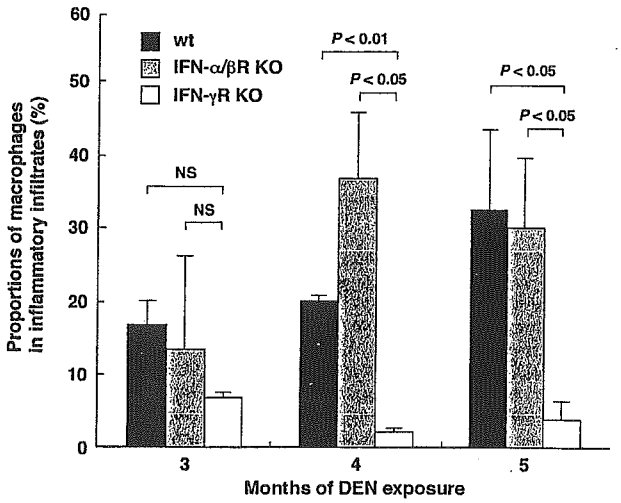

Figure 5 Quantitative immunohistochemical analysis of inflammatory infiltrates in the livers of IFN-γR KO, IFN-α/βR KO, and wt mice after diethylnitrosamine (DEN) exposure. Mice were killed at the time points indicated. Liver samples were stained immunohistochemically with rat monoclonal antibody to mouse macrophage. A total of 100 high-power (× 400) fields representing 4 mm^2 of liver tissue were examined. The proportions (%) of macrophages are expressed as means ± s.e. In contrast to IFN-α/βR KO and wt mice, the proportions of macrophages were greatly reduced in IFN-γR KO mice.

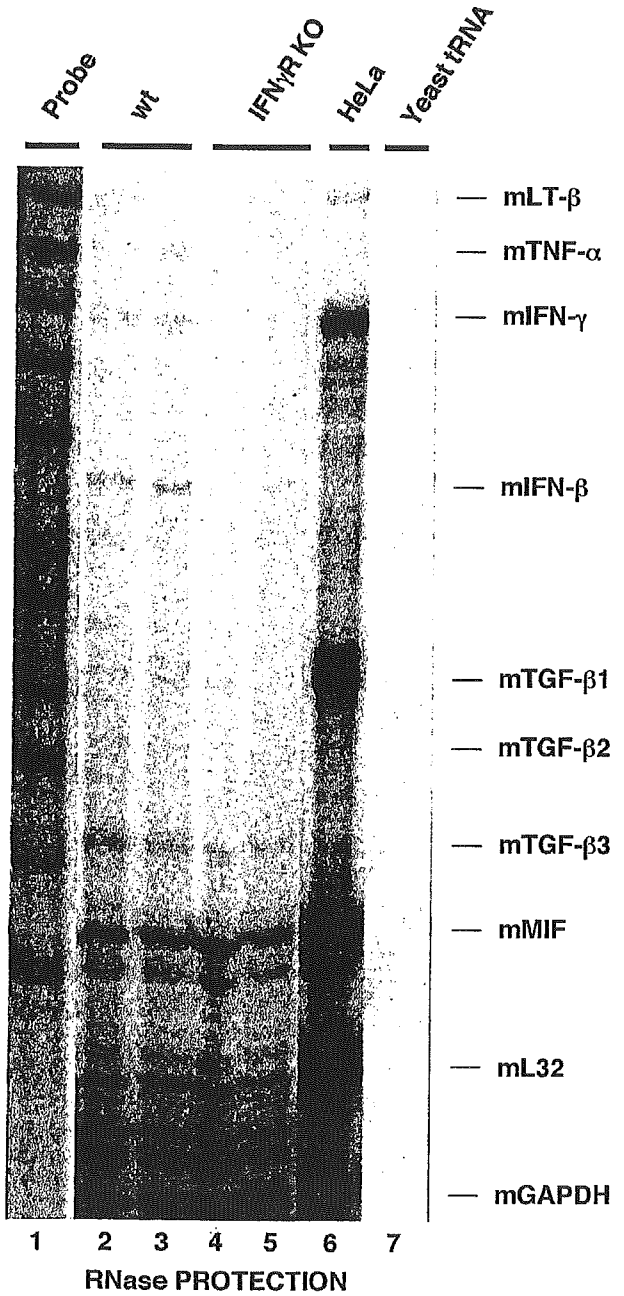

Figure 6 Analysis of intrahepatic cytokine mRNA expression in wt and IFN-γR KO mice after 3 months of diethylnitrosamine (DEN) exposure. Total RNA (15 μg) was extracted from nontumorous liver tissue of representative mice and subjected to RNase protection assay to monitor the expression of a panel of inflammatory cytokines. Intrahepatic expression of LT-β, TNF-α, IFN-γ, IFN-β, and TGF-β3 was weaker in IFN-γR KO mice than in wt mice. The housekeeping genes, ribosomal protein light 32 (L32), and glyceraldehyde-3-phosphate dehydrogenase (GAPDH) were used to normalize the amount of RNA loaded in each lane.

cinogenesis because the proportion of infiltrating macrophages was diminished and the activation status was reduced in IFN-γR KO mice, in which the total numbers of liver tumors were lower than wt mice.

Amounts of 8-OHdG Detected in the Liver

To estimate the oxidative DNA damage in chemical hepatocarcinogenesis, genomic DNA was extracted from nontumorous liver tissue of representative mice treated with DEN for 3 months and subjected to measurement of 8-OHdG by ELISA. Lower amounts of 8-OHdG were detected in the livers of IFN-γR KO mice than of IFN-α/βR KO and wt mice (Figure 7). The results indicate that the oxidative DNA damage caused during DEN exposure period was reduced in IFN-γR KO mice, suggesting that IFN-γ may contribute to the enhancement of the oxidative damage and allow cells that carry damaged DNA to survive in the process of DEN-induced hepatocarcinogenesis.

Discussion

The current study shows that type II IFN, but not type I IFNs, may be involved critically in the initiation stage, but not the promotion stage, of hepatocarcinogenesis in mice treated with DEN. IFN-γR KO mice developed fewer HCCs than IFN-α/βR KO and wt mice, although the diameters of liver tumors were not significantly different among the three lineages. In IFN-γR KO mouse livers, the proportion of monocytes/macrophages was greatly reduced and their activation status was reflected by the lower levels of intrahepatic cytokine expression, suggesting that IFN-γ may contribute to the activation of monocytes/macrophages seen during the process of DEN-induced hepatocarcinogenesis. The activated state of the monocytes/macrophages was

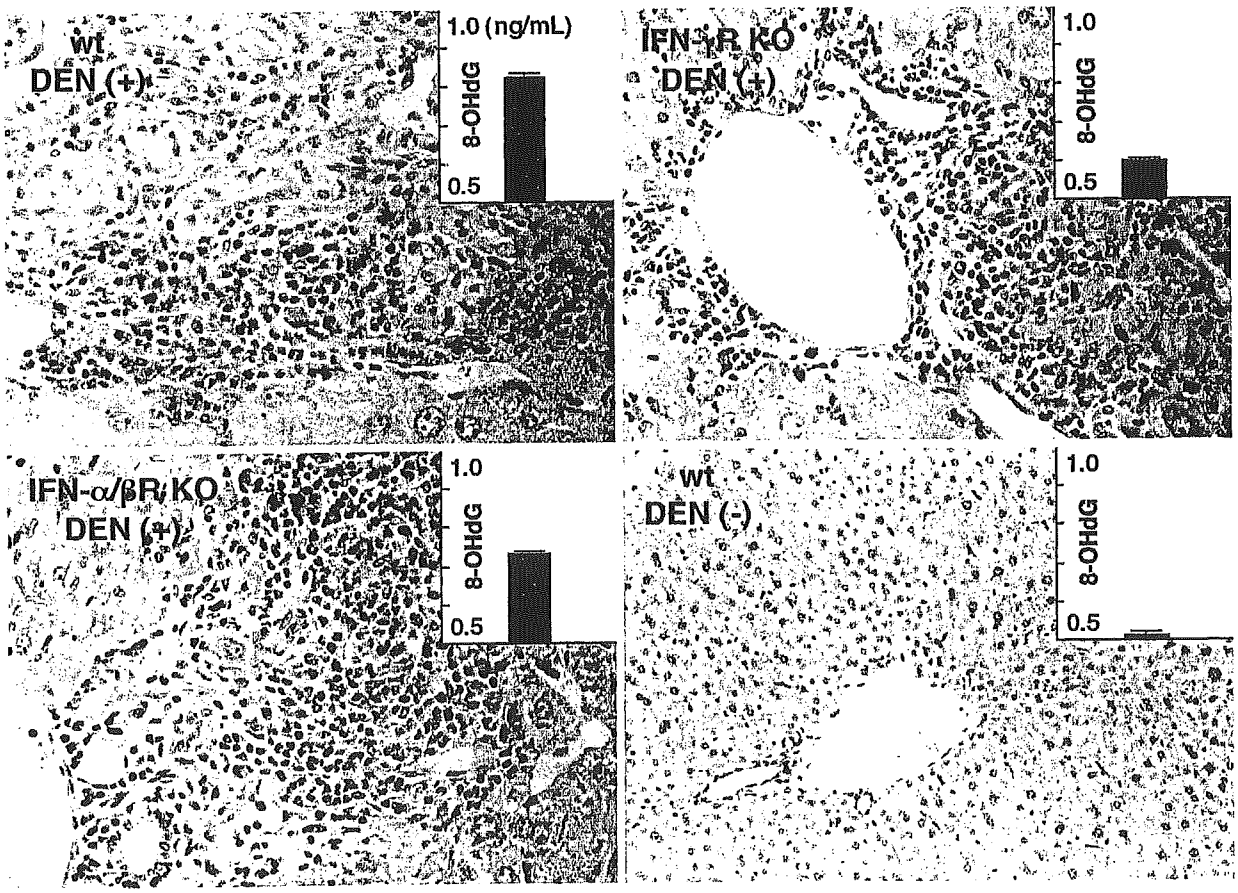

Figure 7 Immunohistochemical analysis of inflammatory infiltrates and 8-hydroxydeoxyguanosine (8-OHdG) amounts detected in the livers of IFN-γR KO, IFN-α/βR KO, and wt mice exposed to diethylnitrosamine (DEN) for 3 months. Liver samples were stained immunohistochemically with rat monoclonal antibody to mouse macrophage (in brown). In contrast to the subsets of infiltrating inflammatory cells in IFN-α/βR KO and wt mice liver, the proportions of macrophages were greatly reduced in IFN-γR KO mice. For measuring 8-OHdG levels, four samples from each strain were used. The amounts of 8-OHdG are expressed as means ± s.e. The amounts of 8-OHdG, indicated in each inset, were in lesser extent in the livers of IFN-γR KO mice than in those of IFN-α/βR KO and wt mice ($P<0.05$).

reflected by the extent of intrahepatic cytokine expression in the mice. Furthermore, on the basis of amounts of 8-OHdG detected, oxidative DNA damage was induced to a lesser extent in livers of IFN-γR KO mice than in those of IFN-α/βR KO and wt mice, leading to a difference in the mutagenic potential and the development of HCC.

The pathogenetic importance of proinflammatory cytokines in DEN-induced hepatocarcinogenesis was evaluated in this study. Intrahepatic IFN-β and IFN-γ mRNA expression, as well as TNF-α, LT-β, TGF-β1, and TGF-β3, were induced after 1 month of DEN exposure and remained high for the period of study. Importantly, the induction of cytokines began 2 months earlier than the appearance of the liver tumors, suggesting that the immune responses may precede the development of HCC during the process of chemical carcinogenesis. Previous studies demonstrated that type I IFNs inhibit the growth of neoplastic cells by inducing apoptosis[15] and that type II IFN is the major proinflammatory cytokine that regulates macrophage function and contributes critically to the establishment of chronic inflammation.[16] However, the pathophysiological role of the cytokines in DEN-induced hepatocarcinogenesis was not well determined.

To define the pathophysiological role of the IFNs in the process of DEN-induced hepatocarcinogenesis, mice genetically deficient for the IFN-α/β or IFN-γ receptor were exposed to DEN, and tumor development was monitored. The results indicate that IFN-γ, but not IFN-α/β, may be involved critically in the initiation stage, but not the promotion stage, of hepatocarcinogenesis in mice treated with DEN. The results are consistent with the reports in which IFN-γ was suggested to promote tumor initiation of cholangiocarcinoma and lung cancer by causing activation of inducible nitric oxide synthase (iNOS) and excess production of nitric oxide (NO), increased manganese superoxide dismutase (Mn-SOD) and decreased catalase, and subsequent DNA damage.[17,18]

Further, in contrast to the subsets of infiltrating inflammatory cells in IFN-α/βR KO and wt mouse livers, the proportion of monocytes/macrophages was greatly reduced in IFN-γR KO mouse livers. The reduction in the percentage of monocytes/macrophages in inflammatory infiltrates in IFN-γR KO mice reflected a deficiency of IFN-γ stimulation because IFN-γ is known to promote macrophage chemotaxis indirectly and to induce its activation directly. Its indirect chemotactic activity is reported to be mediated by macrophage-attracting chemokines, for example, macrophage inflammatory protein (MIP)-1α and monocyte chemoattractant protein (MCP)-1.[19] Recruited and activated macrophages may induce oxidative DNA damage in hepatocytes, probably by NO production,[20,21] which is consistent with our observation that oxidative DNA damage was induced, on the basis of the amounts of 8-OHdG detected, to a lesser extent in the livers of IFN-γR KO mice than in those of IFN-α/βR KO and wt mice.

The current observations emphasize the pathogenetic potential of IFN-γ during the course of chemical hepatocarcinogenesis. Interestingly, IFN-γ influences the initiation stage, which is associated with the recruitment/activation of monocytes/macrophages and the induction of oxidative DNA damage in hepatocytes, and not the promotion stage of hepatocarcinogenesis.

References

1 Colombo M, de Franchis R, Del Ninno E, *et al.* Hepatocellular carcinoma in Italian patients with cirrhosis. N Engl J Med 1991;325:675–680.
2 Okuda K. Hepatocellular carcinoma: recent progress. Hepatology 1992;15:948–963.
3 Ikeda K, Saitoh S, Koida I, *et al.* A multivariate analysis of risk factors for hepatocellular carcinogenesis: a prospective observation of 795 patients with viral and alcoholic cirrhosis. Hepatology 1993;18:47–53.
4 Tsukuma H, Hiyama T, Tanaka S, *et al.* Risk factors for hepatocellular carcinoma among patients with chronic liver disease. N Engl J Med 1993;328:1797–1801.
5 Grisham JW. Interspecies comparison of liver carcinogenesis: implications for cancer risk assessment. Carcinogenesis 1997;18:59–81.
6 Nakamoto Y, Guidotti LG, Kuhlen CV, *et al.* Immune pathogenesis of hepatocellular carcinoma. J Exp Med 1998;188:341–350.
7 Nakamoto Y, Kaneko S, Fan H, *et al.* Prevention of hepatocellular carcinoma development associated with chronic hepatitis by anti-fas ligand antibody therapy. J Exp Med 2002;196:1105–1111.
8 Verna L, Whysner J, Williams GM. *N*-nitrosodiethylamine mechanistic data and risk assessment: bioactivation, DNA-adduct formation, mutagenicity, and tumor initiation. Pharmacol Ther 1996;71:57–81.
9 Corcos D, Defer N, Raymondjean M, *et al.* Correlated increase of the expression of the c-ras genes in chemically induced hepatocarcinomas. Biochem Biophys Res Commun 1984;122:259–264.
10 Beer DG, Schwarz M, Sawada N, *et al.* Expression of H-ras and c-myc protooncogenes in isolated gamma-glutamyl transpeptidase-positive rat hepatocytes and in hepatocellular carcinomas induced by diethylnitrosamine. Cancer Res 1986;46:2435–2441.
11 Smith ML, Yeleswarapu L, Locker J, *et al.* Expression of p53 mutant protein(s) in diethylnitrosamine-induced foci of enzyme-altered hepatocytes in male Fischer-344 rats. Carcinogenesis 1991;12:1137–1141.
12 Johnson SJ, Burr AW, Toole K, *et al.* Macrophage and hepatic stellate cell responses during experimental hepatocarcinogenesis. J Gastroenterol Hepatol 1998;13:145–151.
13 Ahn B, Han BS, Kim DJ, *et al.* Immunohistochemical localization of inducible nitric oxide synthase and 3-nitrotyrosine in rat liver tumors induced by *N*-nitrosodiethylamine. Carcinogenesis 1999;20:1337–1344.
14 Ikeda T, Nishimura K, Taniguchi T, *et al. In Vitro* Evaluation of drug interaction caused by enzyme inhibition-HAB protocol. Xenobio Metabol Dispos 2001;16:115–126.

15 Kayagaki N, Yamaguchi N, Nakayama M, *et al.* Type I interferons (IFNs) regulate tumor necrosis factor-related apoptosis-inducing ligand (TRAIL) expression on human T cells: a novel mechanism for the antitumor effects of type I IFNs. J Exp Med 1999;189: 1451–1460.
16 Toyonaga T, Hino O, Sugai S, *et al.* Chronic active hepatitis in transgenic mice expressing interferon-gamma in the liver. Proc Natl Acad Sci USA 1994;91: 614–618.
17 Jaiswal M, LaRusso NF, Burgart LJ, *et al.* Inflammatory cytokines induce DNA damage and inhibit DNA repair in cholangiocarcinoma cells by a nitric oxide-dependent mechanism. Cancer Res 2000;60: 184–190.
18 Chung-man Ho J, Zheng S, Comhair SA, *et al.* Differential expression of manganese superoxide dismutase and catalase in lung cancer. Cancer Res 2001; 61:8578–8585.
19 Warhurst AC, Hopkins SJ, Warhurst G. Interferon gamma induces differential upregulation of alpha and beta chemokine secretion in colonic epithelial cell lines. Gut 1998;42:208–213.
20 Gal A, Tamir S, Kennedy LJ, *et al.* Nitrotyrosine formation, apoptosis, and oxidative damage: relationships to nitric oxide production in SJL mice bearing the RcsX tumor. Cancer Res 1997;57:1823–1828.
21 Zhuang JC, Lin C, Lin D, *et al.* Mutagenesis associated with nitric oxide production in macrophages. Proc Natl Acad Sci USA 1998;95:8286–8291.

Int. J. Cancer: **114**, 209–218 (2005)

Aberrant expression of serine/threonine kinase Pim-3 in hepatocellular carcinoma development and its role in the proliferation of human hepatoma cell lines

Chifumi Fujii[1,2], Yasunari Nakamoto[3], Peirong Lu[1], Koichi Tsuneyama[4], Boryana K. Popivanova[1], Shuichi Kaneko[3] and Naofumi Mukaida[1,2]*

[1]*Division of Molecular Bioregulation, Cancer Research Institute, Kanazawa University, Kanazawa, Ishikawa*
[2]*Center for the Development of Molecular Target Drugs, Cancer Research Institute, Kanazawa University, Kanazawa, Ishikawa*
[3]*Department of Gastroenterology, Graduate School of Medical Science, Kanazawa University, Kanazawa, Ishikawa*
[4]*Department of Surgical Pathology, Toyama Medical and Pharmaceutical University Hospital, Toyama, Japan*

Most cases of human hepatocellular carcinoma develop after persistent chronic infection with human hepatitis B virus or hepatitis C virus, and host responses are presumed to have major roles in this process. To recapitulate this process, we have developed the mouse model of hepatocellular carcinoma using hepatitis B virus surface antigen transgenic mice. To identify the genes associated with hepatocarcinogenesis in this model, we compared the gene expression patterns between pre-malignant lesions surrounded by hepatocellular carcinoma tissues and control liver tissues by using a fluorescent differential display analysis. Among the genes that were expressed differentially in the pre-malignant lesions, we focused on Pim-3, a member of a proto-oncogene *Pim* family, because its contribution to hepatocarcinogenesis remains unknown. Moreover, the unavailability of the nucleotide sequence of full-length human *Pim-3* cDNA prompted us to clone it from the cDNA library constructed from a human hepatoma cell line, HepG2. The obtained 2,392 bp human *Pim-3* cDNA encodes a predicted open reading frame consisting of 326 amino acids. Pim-3 mRNA was selectively expressed in human hepatoma cell lines, but not in normal liver tissues. Moreover, Pim-3 protein was detected in human hepatocellular carcinoma tissues and cell lines but not in normal hepatocytes. Furthermore, cell proliferation was attenuated and apoptosis was enhanced in human hepatoma cell lines by the ablation of *Pim-3* gene with RNA interference. These observations suggest that aberrantly expressed Pim-3 can cause autonomous cell proliferation or prevent apoptosis in hepatoma cell lines.

Key words: protein serine-threonine kinases; pre-malignant lesions; hepatocellular carcinoma; RNA interference; apoptosis

Hepatocellular carcinoma (HCC) is the 8th highest cause of death among human cancers and is endemic in Asia, Africa and southern Europe. Most cases of HCC arise from persistent chronic infection with human hepatitis B virus (HBV) or hepatitis C virus (HCV).[1] Host responses are presumed to be involved in the development of HCC among patients harboring HBV or HCV, because these viruses lack apparent oncogenes and the infected patients develop HCC after suffering from chronic hepatitis-related pathology.[2,3]

Hepatitis virus infection induces the generation of virus antigen-specific cytotoxic T lymphocytes, which have been implicated in both the eradication of viruses and liver injury.[4] Cycles of cytotoxic T lymphocyte-mediated liver cell destruction and regeneration are thought to prepare the mitogenic environment.[4,5] To elucidate the molecular and cellular mechanism of HCC initiation and development, Nakamoto *et al.*[6] has established a mouse model of HCC by using HBV surface antigen (HBsAg) transgenic mice (HBsTg). In this model, bone marrow cells and splenocytes were obtained from syngeneic wild-type mice, which were immunized with HBsAg and were transplanted into HBsTg mice, which were irradiated beforehand. At 15 months after the transplantation, the transgenic mice developed multiple foci of HCC surrounded by non-malignant areas consisting of hepatocytes with atypical nuclear configuration.[6,7]

To obtain the molecular insights on hepatocarcinogenesis, we compared the gene expression pattern between non-tumor portion of this model as a pre-malignant lesion and normal tissues by using a fluorescent differential display (FDD) analysis. We observed that several genes are expressed differentially in this pre-malignant lesion, compared to normal liver tissues. Of interest is that the gene expression of Pim-3, originally identified as depolarization-induced gene in a rat pheochromocytoma cell line,[8] was enhanced in this pre-malignant lesion. We demonstrated that Pim-3 was expressed aberrantly in human HCC tissues and hepatoma cell lines but not normal liver tissues. We also provided evidence to suggest the involvement of Pim-3 in the proliferation of human hepatoma cell lines.

Material and methods

Experimental animals

HBsAg transgenic mouse lineage 107-5D (official designation Tg[Alb-1,HBV]Bri66; inbred B10D2, H-2^d) was provided by Dr. F.V. Chisari (The Scripps Research Institute, La Jolla, CA).[9] Lineage 107-5D contains the entire HBV envelope-coding region (subtype ayw) under the transcriptional control of the mouse albumin promoter, and expresses the HBV small, middle and large envelope proteins in their hepatocytes.[9] They display no evidence of liver disease during their lifetime unless they receive the adoptive transfer of HBsAg-specific cytotoxic T lymphocytes,[9] due to their immunological tolerance to the HBs transgene at the T cell level.[10]

Chronic hepatitis-related liver disease model was generated as described previously.[6] Briefly, after male HBsAg transgenic mice were thymectomized and irradiated (900 cGy), their hematopoietic system was reconstituted with the bone marrow cells from syngeneic non-transgenic B10D2 (H-2^d) mice. At 1 week after the bone marrow transplantation, the animals received 10^8 splenocytes from syngeneic non-transgenic B10D2 (H-2^d) mice that were infected intraperitoneally with a recombinant vaccinia virus expressing HBsAg 3 wk before the splenocyte transfer. At 12–15 months after the lymphocyte transfer, multiple HCC foci developed in mice.[6,7] Non-tumor and tumor portions were demarcated macroscopically and were removed separately. A pathologist without a prior knowl-

DNA Data Bank of Japan Accession Number AB114795.

Abbreviations: BSA, bovine serum albumin; DMEM, Dulbecco's modified Eagle's medium; FBS, fetal bovine serum; FDD, fluorescent differential display; GAPDH, glyceraldehyde 3-phosphate dehydrogenase; HBV, hepatitis B virus; HCV, hepatitis C virus; HBs, HBV surface; HBsAg, HBV surface antigen; HBsTg, HBs transgenic mice; HCC, hepatocellular carcinoma; IL, interleukin; PBS (−), phosphate buffered saline; PCR, polymerase chain reaction; RNAi, RNA interference; RT-PCR, reverse transcription-polymerase chain reaction; siRNA, short interfering RNA; STAT, signal transducers and activators of transcription; VCP, valosine-containing protein.

***Correspondence to:** Division of Molecular Bioregulation, Cancer Research Institute, Kanazawa University, 13-1 Takara-machi, Kanazawa, Ishikawa 920-0934, Japan. Fax: +81-76-234-4520.
E-mail: naofumim@kenroku.kanazawa-u.ac.jp
Received 14 May 2004; Accepted after revision 1 September 2004
DOI 10.1002/ijc.20719
Published online 11 November 2004 in Wiley InterScience (www.interscience.wiley.com).

Publication of the International Union Against Cancer

edge on the experimental procedures confirmed the presence of hepatocytes with atypical configurations but not malignant cells in this non-tumor potion. Non-tumor portions were designated as pre-malignant lesions in the following experiments. Liver tissues were also obtained from untreated or HBsTg mice transplanted with tolerant splenocytes as a control.

Fluorescent differential display

Total RNAs extracted from liver tissues were subjected to FDD according to the method described by Ito et al.[11] Briefly, total RNAs were isolated with RNA-Bee (Tel-Test, Inc., Friendswoods, TX), followed by the treatment with RNase-free DNase (Takara Shuzo, Kyoto, Japan). The purified total RNAs (2.5 μg) were reverse-transcribed with SuperScript II reverse transcriptase (Invitrogen, Carlsbad, CA) and fluorescein-labeled anchor primer, $GT_{15}A$, $GT_{15}C$ or $GT_{15}G$. The resultant cDNA equivalent to 50 ng of RNA was subjected to polymerase chain reaction (PCR) with 0.5 μM anchor primer, 0.5 μM arbitrary primer (10 mer kit A; Operon Biotechnology, Huntsville, AL), 50 μM each dNTP, 1 unit of *Gene Taq* DNA polymerase (Nippon Gene, Toyama, Japan), and 1 U of *Taq* DNA polymerase (Takara Shuzo). PCR products were separated with 6% polyacrylamide-8 M urea gel and analyzed by employing Vistra Fluor Imager SI (Molecular Dynamics, Sunnyvale, CA). The bands of interest were excised from the gel and cloned into pSTBlue-1 Vector (Novagen, San Diego, CA). The inserted cDNA was sequenced with CEQ 2000 DNA Analysis System (Beckman Coulter, Fullerton, CA) and analyzed with the BLAST program to search the GenBank database.

Cell culture

Human hepatoma cell lines (HepG2, Hep3B, HLE, HLF, HuH7 and SK-Hep1) were maintained in DMEM (Sigma-Aldrich, St. Louis, MO) supplemented with 10% heat-inactivated FBS (Atlanta Biologicals, Norcross, GA) at 37°C in a humidified atmosphere with 5% CO_2 in the air.[12]

Semi-quantitative RT-PCR

Total RNAs were isolated with RNA-Bee, followed by the treatment with RNase-free DNase (Takara Shuzo), and a semi-quantitative RT-PCR analysis was carried out as described previously.[13] The cDNA was amplified using the sets of the primers that specifically amplify *Pim* family kinases and glyceraldehyde 3-phosphate dehydrogenase (GAPDH). The sequences are as follows; *Pim-1*, sense 5′-CCCGAGCTATTGAAGTCTGA-3′, antisense 5′-CTGTGCAGATGGATCTCAGA-3′; *Pim-2*, sense 5′-CATCCCCAGCAGCTCTTTAG-3′, antisense 5′-CAGTAGGGTCCCTCACCAAA-3′; *Pim-3*, sense 5′-AAGCAGTGACCTCTGACCCCTGGTGACC-3′, antisense 5′-CAGCGGAACCGCTCATTGCCAATGG-3′; GAPDH, sense 5′-ACCACAGTCCATGCCATCAC-3′, antisense 5′-TCCACCACCCTGTTGCTGTA-3′. The resultant PCR products were separated on 1.5% agarose gel and visualized by ethidium bromide staining. The band intensities were measured using NIH Image Analysis Software Ver 1.61 (National Institutes of Health, Bethesda, MD) and the ratios to GADPH were calculated.

cDNA library construction and screening

Total RNA was isolated from HepG2 cell line and polyA mRNA was further separated from total RNA by *Oligotex-dT30* mRNA Purification kit (Takara Shuzo). cDNA was synthesized with SuperScript II reverse transcriptase (Invitrogen) and oligo-dT primer, and cDNA library was constructed in pCMVSPORT6 (Invitrogen) with *Escherichia coli* DH10B (Invitrogen), according to the manufacturer's instructions. The initial screening was carried out using GENE TRAPPER® cDNA Positive Selection System (Invitrogen) and the oligomer, CTGTGAAGCACGTGGTGAAG, as a probe. The obtained colonies were subjected to colony PCR screening with the sets of primers described above. The inserted cDNA was sequenced with CEQ 2000 DNA Analysis System (Beckman Coulter).

Northern blot analysis

Human *Pim-3* mRNA expression was analyzed by using Human 12-Lane MTN Blot (Clontech, Palo Alto, CA). *In vitro* transcribed digoxigenin-labeled probes were hybridized overnight at appropriate temperatures (70°C for *Pim-3* and 68°C for *GAPDH*). After being washed sequentially each for 15 min in 2× and 0.5× SSC buffer containing 0.1% sodium dodecyl sulfate at room temperature and at 68°C, respectively, the hybridized probes were detected by the DIG detection kit (Boehringer Mannheim Biochemicals, Mannheim, Germany), according to the manufacturer's instructions.

Preparation of anti-Pim-3 polyclonal antibodies

Anti-Pim-3 antibodies were prepared by Asahi Techno Glass Co. (Tokyo, Japan). Briefly, chickens were immunized with keyhole limpet hemocyanin-conjugated Pim-3 peptide, CGPGGVDHLPVKILQPAKAD, which corresponds to the amino acid residues between 13–32 in human Pim-3 and is conserved in murine Pim-3, and their egg yolks were harvested before and after the immunization. IgY proteins were purified with EGGstract IgY Purification System (Promega, Madison, WI) according to the manufacturer's instructions. They were affinity-purified with Pim-3 peptide conjugated NHS-activated HP (Amersham Biosciences, Tokyo, Japan). Purified antibodies were quantified by measuring the absorbance at 280 nm.

Immunohistochemical analysis

Human liver specimens were surgically obtained from the patients with their informed consent. Mouse liver tissues were obtained from HBsTg mouse at the indicated time intervals after splenocyte transfer. Paraffin-embedded tissue sections were deparaffinized in xylene and rehydrated through graded concentrations of ethanol (70–100%). After incubation with 0.3% hydrogen peroxide in 10 mM phosphate buffer, pH 7.4, containing 150 mM NaCl (PBS [−]), sections were incubated sequentially with 3% normal rabbit serum (DAKO, Kyoto, Japan) and 2% BSA in PBS (−) and with Avidin-Biotin blocking kit (Vector Laboratories, Burlingame, CA). Slides were treated subsequently with 10 μg/ml anti-Pim-3 IgY or pre-immunized IgY at 4°C overnight, followed by the incubation with 2.5 μg/ml biotin-conjugated rabbit anti-chicken IgY antibodies (Promega) at room temperature for 30 min. The immune complexes were visualized by using the Vectastain Elite ABC kit (Vector Laboratories) and Vectastain DAB substrate kit (Vector Laboratories) according to the manufacturer's instructions. The slides were counterstained with hematoxylin (DAKO), mounted, and observed under a microscope (BX-50; Olympus, Tokyo, Japan).

Immunocytochemical analysis of HuH7 cells

Cells were cultured on Lab-Tec chamber slides (Nalge Nunc, Roskilde, Denmark). They were fixed with 4% paraformaldehyde in PBS (−) and permeated in methanol. Then, they were blocked by incubation with 3% normal rabbit serum and 2% BSA in PBS (−) at room temperature for 30 min, and with Avidin-Biotin blocking kit. They were treated subsequently with 20 μg/ml affinity-purified anti-Pim-3 IgY or pre-immunized IgY at 4°C overnight, with 2.5 μg/ml biotin-labeled rabbit anti-chicken IgY at room temperature for 30 min. The signals were amplified and visualized by the Vectastain Elite ABC kit and Vectastain DAB substrate kit according to the manufacturer's instructions. The slides were counterstained with methyl green (DAKO), mounted, and observed under a microscope (BX-50; Olympus).

RNA interference

Short interfering RNA (siRNA) was synthesized with *Silencer* siRNA Construction Kit (Ambion, Austin, TX) according to the manufacturer's instructions. By employing siRNA Target Finder and Design Tool (Ambion), siRNA duplexes were designed to target $AA(N_{19})UU$ sequences in the open reading frame of mRNA encoding *Pim-3*. The selected siRNA target sequence (5′-

TABLE I – IDENTIFICATION OF GENES DIFFERENTIALLY EXPRESSED IN PRE-MALIGNANT LESION OF HBsTg MICE

Classification	Description	Accession number
Upregulated		
Transcription factors	Y box protein 3	AK029441
Immune system proteins	Complement component 3	BC043338
Xenobiotic metabolism	Ceruloplasmin	NM_00775
	Metallothionein II	AK002567
Oncogenes	24p3 (lipocalin 2)	X81627
Metabolism enzymes	Aldehyde dehydrogenase family 1, subfamily A1	BC044729
	Hemoglobin α, adult chain 1	NM_008218
	Phosphoenolpyruvate carboxy-kinase 1	NM_011044
	Succinate dehydrogenase complex, subunit A flavoprotein	BC031849
Growth factors, cytokines, and chemokines	Growth differentiation factor 15 (macrophage inhibiting compound-1)	NM_011819
	Insulin-like growth factor binding protein 1	NM_008341
Non-receptor protein kinases	Serine/threonine kinase pim-3	NM_145478
Not classified	BetaKlotho	AF178429
	Pol protein	XM_196572
	Serine (or cysteine) proteinase inhibitor, clade A, member 6	NM_007618
Putative proteins	Hypothetical Esterase/acetylhydrolase structure containing protein	NM_026347
	Putative el protein	AK090127
	Similar to bile acid Coenzyme A: amino acid N-acyltransferase	NM_145368
Est		AW047153
		BE132832
		BB168703
		BM224373
Unknown	Fibronectin non-coding region	
	Hypothetical protein non-coding region chromosome 5	
Downregulated		
Immune system proteins	β2-microglobulin	M84367
	Complement component CISA	AF459017
Extracellular transport/carrier proteins	Serum amyloid A-1	M13521
Metabolism enzymes	Cytochrome P450 4A10	BC031141
	Hemoglobin β, adult major chain	AK027904
	Stearoyl-Coenzyme A desaturase 1	BC007474
	Isocitrate dehydrogenase 1 (NADP+), soluble	AK087063
Not classified	Endogenous retrovirus 3′ LTR	K02892
	Glutatione S-transferase	BC009805
	Group 1 major urinary protein	X03208
	Major urinary protein 1	BC012221
	Major urinary protein 2	BC012259
	Major urinary protein 3	XM_135398
	Major urinary protein 11 and 8	AK011413
	Preimplantation protein 2	AK028563
	Ubiquitin-associated protein 1	NM_023305
Mitchondrial gene	Cytochrome oxidase A1	V00711
Putative proteins	Archerase	AY071852
	Dis3 protein homolog	AK032091

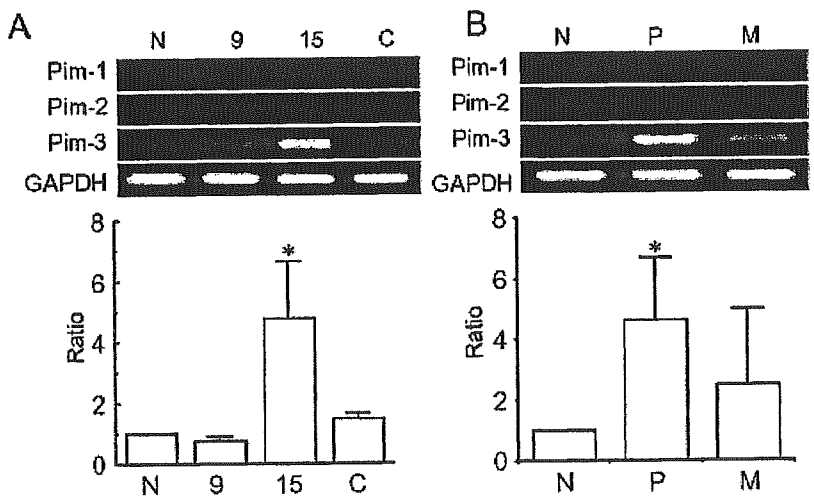

FIGURE 1 – Semi-quantitative RT-PCR analysis for proto-oncogene *Pim* family mRNA expression in HBsTg mice. (*a*) Total RNAs were extracted from HBsTg ice before (N), 9 (whole liver, 9), 15 months (pre-malignant lesions, 15) after splenocyte transfer, or transgenic splenocytes transfer (C). (*b*) Total RNAs were extracted from pre-malignant (P) or malignant (M) tissues of HBV transgenic mice 15 months after splenocyte transfer. Representative results from 3 independent experiments are shown in the upper panels. The ratios of the PCR product for Pim-3 to GAPDH were determined, and relative intensities were calculated to assume the ratio of untreated mice as 1.0. Means and SD were calculated and are shown in the lower panels. Statistical significance was evaluated using ANOVA test, and $p < 0.05$ was accepted as statistically significant. $*p < 0.05$ compared to N.

GCACGUGGUGAAGGAGCGG-3′ corresponding to 642–661) was further subjected to BLAST searches against other human genome sequences to ensure its target specificity. We identified 2 distinct cDNAs, which exhibit identity with the target sequence at 16 of 19 nucleotides. We could not, however, detect any specific bands corresponding to these cDNAs in HuH7 and Hep3B cell

lines by RT-PCR analysis (our unpublished data), further indicating the specificity of the used target sequence. Scramble siRNA (5′-GCGCGCUUUGUAGGAUUCG-3′ designed by B-Bridge International, Inc.) was used as a negative control. Each siRNA duplex (final concentration 50 nM) was mixed with 12.5 μl and 12 μl of Lipofectamine 2000 (Invitrogen) for HuH7 and Hep3B, respectively. The mixtures were added into 2.5 ml of Opti-MEM (Invitrogen) and allowed to stand at room temperature for 20 min. The final mixture was then added directly into the semi-confluent cells in 6-cm culture dishes, which were washed with serum-free DMEM beforehand. The following day, 2.5 ml of DMEM plus 20% FBS medium was added to adjust the FBS concentration to 10%. At the indicated time intervals, cells were harvested for further analyses.

Semi-quantitative RT-PCR analysis of siRNA transfectant

Hep3B and HuH7 cells were harvested at 2 and 4 days after the transfection, respectively. Total RNAs were extracted and a semi-quantitative RT-PCR analysis was carried out as described above. The cDNA was amplified using the sets of the primers that specifically amplify *Pim-3* (sense 5′-ATGCTGCTCTCCAAGTTC-GGCTCCCTGGCG-3′, antisense 5′- TCCTGTGCCGGCTCG-GGTCGCTCCAGCACC-3′) and *GAPDH*.

Cell proliferation assay

Cells were trypsinized at 2 days after the transfection, and 5×10^3 cells were plated to each well of 96-well plate. This time point was designated as Day 0. The cell viability was determined every day using WST-1 reagent (an MTT analog from Boehringer-Mannheim Biochemicals) according to the manufacturer's instructions. The ratios to Day 0 were calculated.

Cell-cycle analysis by a flow cytometry

HuH7 cells were harvested at 4 days after the transfection and fixed with graded concentrations of ethanol on ice. They were incubated with 50 μg/ml propidium iodide and 1 μg/ml of RNase A for 30 min at room temperature and quenched by adding EDTA to a final concentration of 10 μM. The filtered cells were analyzed using a FACSCalibur (Becton Dickinson, Bedford, MA). The distribution in each cell-cycle phase was determined by using Cell Quest analysis software (Becton Dickinson).

Chromatin condensation analysis by Hoechst 33258

HuH7 and Hep3B cells were harvested at 4 days after the transfection and stained with Hoechst 33258 to detect the cells with condensed nuclei under a fluorescence microscope (BX-50; Olympus).

Results

Identification of the genes differentially expressed in pre-malignant liver tissue

We compared the gene expression patterns between pre-malignant lesions and normal liver tissues by employing a FDD method. The determination of the nucleotide sequence of the resultant bands identified 24 and 19 distinct genes among the upregulated and downregulated bands in pre-malignant lesions, respectively (Table I). Among these genes, Pim-3 expression has not been reported in normal hepatocytes. We focused on Pim-3, a member of proto-oncogene *Pim* family including Pim-1 and Pim-2. A semi-quantitative RT-PCR analysis confirmed that *Pim-3* mRNA expression was significantly enhanced in the pre-malignant tissues

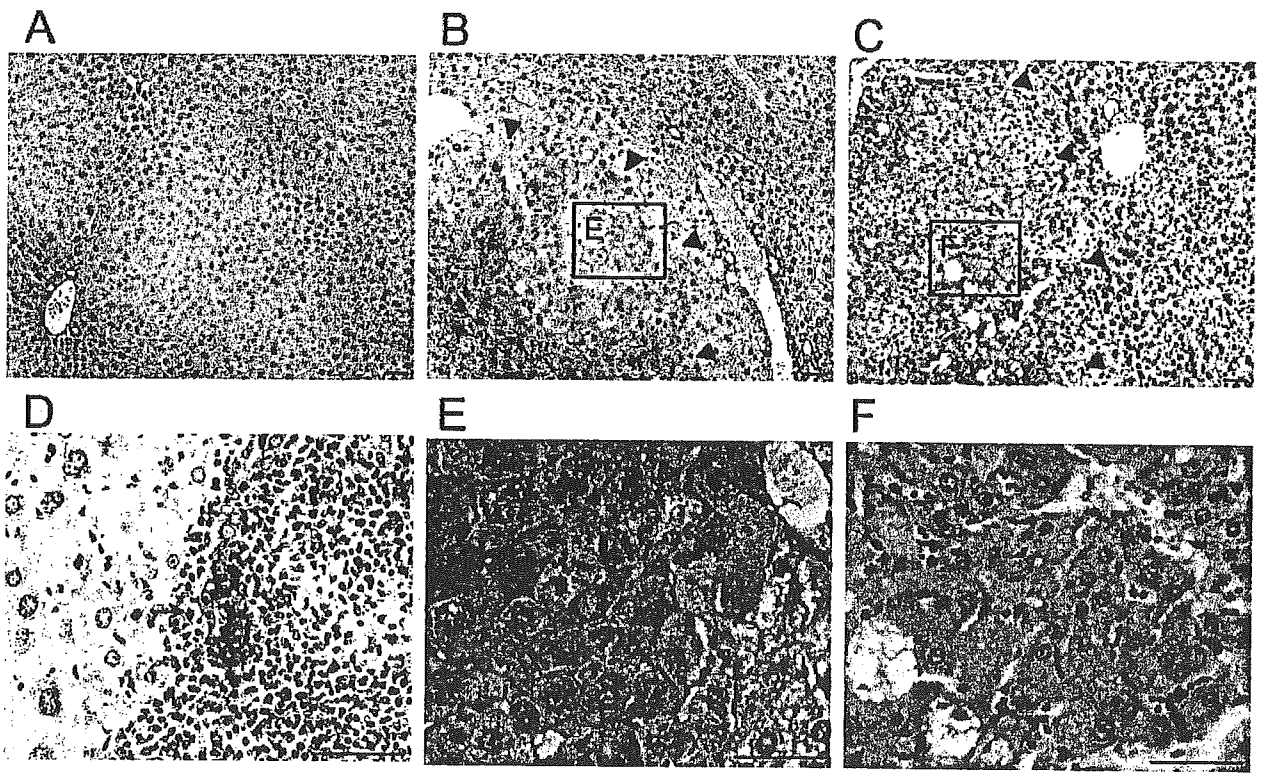

FIGURE 2 – Immunohistochemical analysis of Pim-3 in HBsTg mice. HBsTg mice liver tissues before (*a*) and 15 months after splenocyte transfer (*b,d,e*: non-tumor portions; *c,f*: tumor potions) were immunostained by anti-Pim-3 IgY as described in Material and Methods. Representative results are shown here. (*b*) Pre-malignant lesion is indicated with arrowheads. (*c*) Tumor portion is indicated with arrowheads. (*d*) Positively-stained regenerated proliferating bile ductule. The arrow indicates regenerated proliferating bile ductule. (*e,f*) Positively-stained hepatocytes at a higher magnification of the square in (*b*) and (*c*). Original magnification = (*a–c*) ×100; (*d–f*) ×400. Scale bars = 50 μm.

and to a lesser degree, in HCC tissues, compared to control (Fig. 1). In contrast, specific *Pim-1* and *Pim-2* transcripts were barely detected under these conditions (Fig. 1). These results indicate that *Pim-3* mRNA expression is enhanced during HCC development in this model.

We further localized Pim-3 protein immunohistochemically in liver tissues obtained from HBsTg mouse after splenocyte transfer. We failed to detect Pim-3 protein in unmanipulated mice (Fig. 2*a*) or 9 months after splenocyte transfer, when hepatocytes with atypical nuclear configuration were not detected (data not shown). On the contrary, Pim-3 protein was weakly detected in the cytoplasm of hepatocytes with atypical nuclear configurations in premalignant lesion (Fig. 2*b,e*) and highly differentiated neoplastic hepatocytes in the tumor portion[7] (Fig. 2*c,f*). Moreover, Pim-3

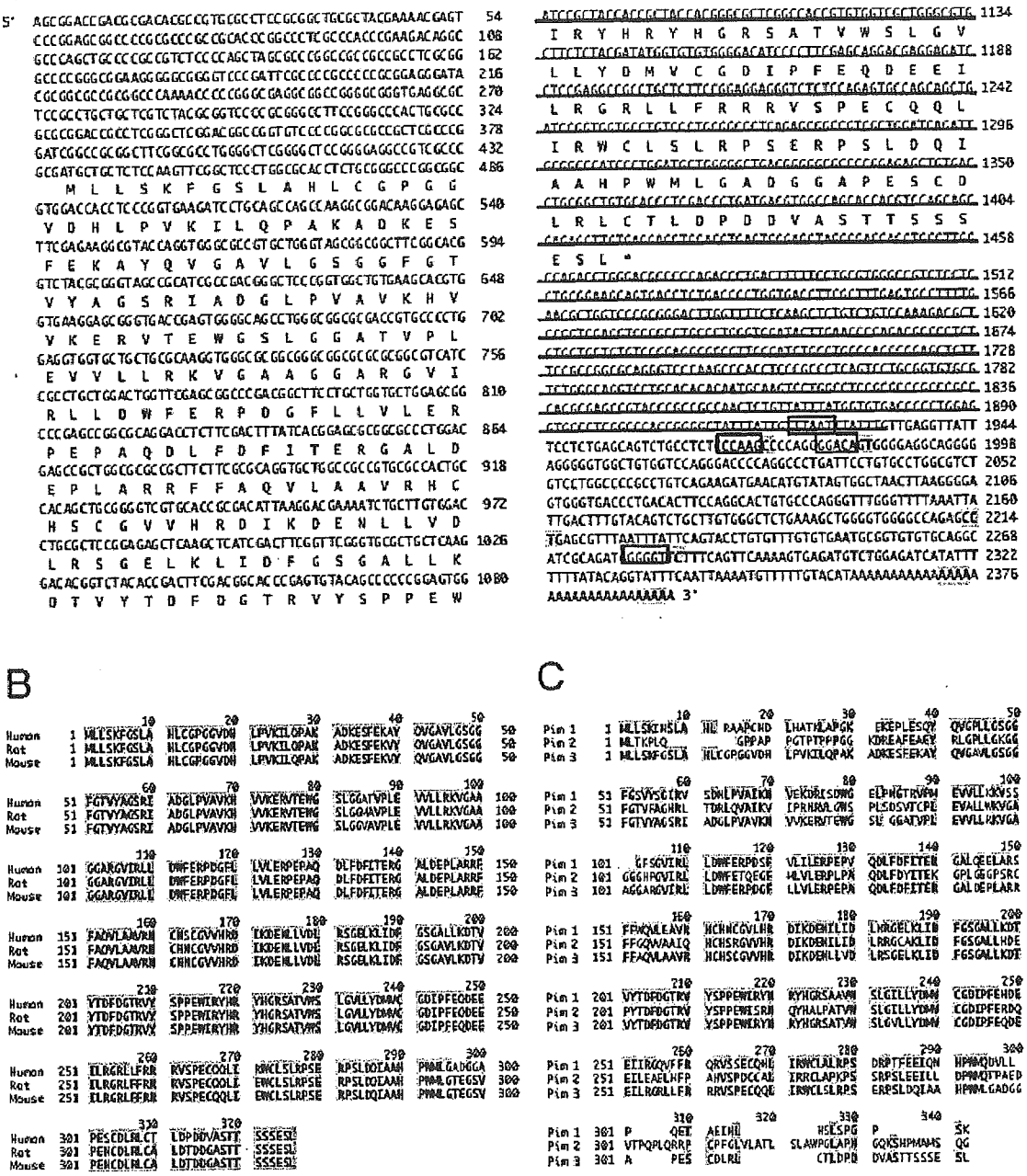

FIGURE 3 – (*a*) Structure of human *Pim-3* cDNA. The nucleotide and predicted amino acid sequences of human Pim-3 are shown. The nucleotide sequence is numbered. The predicted amino acid sequence is shown in a single-letter code below the nucleotide sequence. The AT-rich motifs are indicated in boxes and highlights. The region used as the probe for Northern blot analysis is underlined. (*b,c*) Amino acid alignment of *Pim* family proteins. The amino acid sequences of human, rat, and mouse Pim-3s (*b*) or other members of human *Pim* family kinases (*c*) were aligned using DNASIS-Mac version 3.0 software (Hitachi Software Engineering Co., Ltd., Yokohama, Japan). The residues identical to human Pim-3 are highlighted.

protein was detected in regenerated proliferating bile ductules (Fig. 2*d*, arrow), which are assumed to be the proliferation of hepatic stem cells after chronic liver injuries (*i.e.*, infection, tumors).[14] These results may indicate that Pim-3 protein expression was aberrantly enhanced in liver during the course of hepatocarcinogenesis in this model.

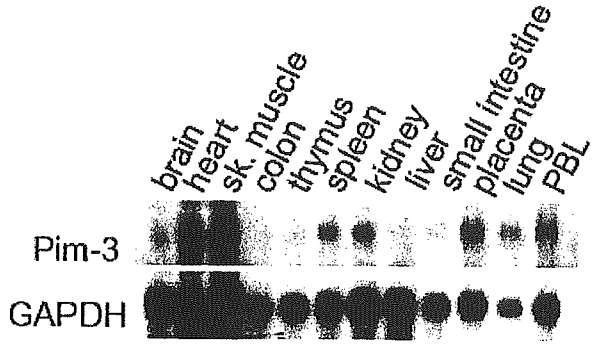

FIGURE 4 – Human *Pim-3* mRNA expression in human normal tissues. Northern blot analysis was carried out as described in Material and Methods. Representative results are shown. sk, muscle, skeletal muscle; PBL, peripheral blood leukocytes. GAPDH mRNA expression was analyzed in parallel to evaluate the amount of mRNA loaded in each lane.

Cloning and determination of nucleotide sequence of human Pim-3

Because the full length human *Pim-3* cDNA nucleotide sequence has not been determined yet, we initially cloned and determined the nucleotide sequence of human *Pim-3* cDNA by screening cDNA library constructed from a human hepatoma cell line, HepG2. Three positive clones were obtained after 2 rounds of screening, and these 3 distinct cDNA clones contained the same insertion consisting of 2,392 bp. The 5′-untranslated region is 82.3% G and C, whereas the 3′-untranslated region contains 5 copies of the ATTTA motif and 8 copies of TATT motif (Fig. 3*a*). This sequence exhibits an identity with a partial human *Pim-3* cDNA sequence predicted from EST database (data not shown).[15] Its open reading frame encodes the protein consisting of 326 amino acids with a calculated molecular weight of 35,861 (Fig. 3*a*). Moreover, the amino acid sequence of the predicted open reading frame, shares a high degree of identity with the mouse[16] and rat Pim-3 (KID-1)[8] proteins (95.0%; Fig. 3*b*). Based on these results, we judged this clone as human *Pim-3* cDNA. Human Pim-3 protein showed a high sequence identity with the quail qPim[17] (73.9%) and *Xenopus* Pim (Pim-1)[18] (68.7%) at the amino acid level (data not shown). Moreover, human Pim-3 protein shows a high sequence identity with human Pim-1[19] (57.1%) and Pim-2[20] (44.0%) at the amino acid level (Fig. 3*c*). Northern blotting analysis detected 2.4-kb mRNA in various organs including heart, skeletal muscle, brain, spleen, kidney, placenta, lung and peripheral blood leukocytes (Fig. 4). In contrast, no specific band was detected in colon, thymus, liver and small intestine under the present experimental conditions (Fig. 4).

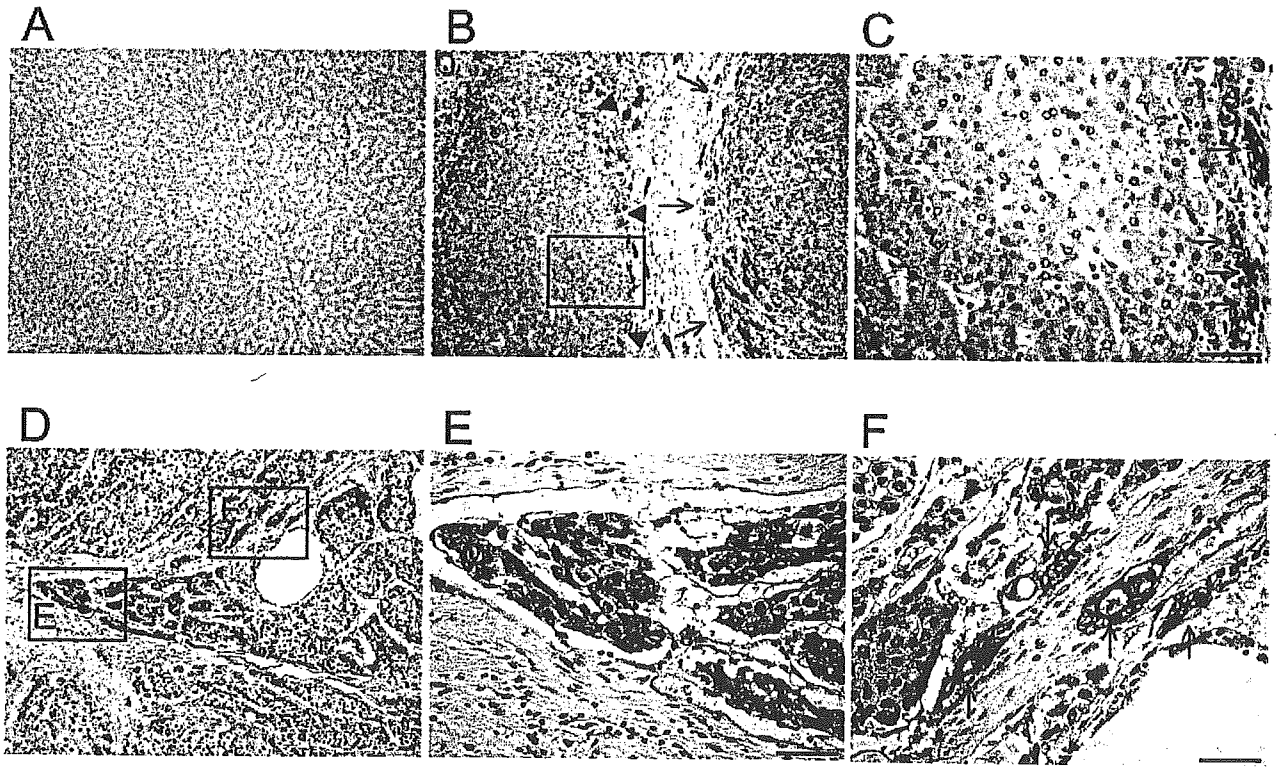

FIGURE 5 – Immunohistochemical analysis of Pim-3 in HCC tissues. Human normal liver tissue (*a*) or HCC tissues (*b–f*) were immunostained by anti-Pim-3 IgY as described in Material and Methods. Representative results are shown. (*b*) Precancerous lesions. The lesions surrounded with arrowheads and arrows are precancerous lesions and HCC lesions, respectively. (*c*) Precancerous lesion in the square of (*b*) is shown at a higher magnification. Arrows indicate regenerated proliferating bile ductules. (*d,e*) Positively-stained HCC cells. (*e*) Indicates the square in (*d*) at a higher magnification. (*f*) Positively-stained regenerated proliferating bile ductules at a higher magnification of the square in (*d*). Arrows indicate regenerated proliferating bile ductules. Original magnification: (*a,b,d*) 100; (*c,e,f*) ×400. Scale bars = 50 μm.

Pim-3 is expressed aberrantly in human HCC

Immunohistochemical analysis failed to detect Pim-3 protein in normal liver tissues (Fig. 5*a*), consistent with the Northern blotting analysis. On the contrary, Pim-3 protein was weakly but diffusely detected in most of large regenerative nodules and adenomatous hyperplasia, lesions with precancerous potential, which were located adjacent to HCC areas (19 of 27 cases; Fig. 5*b,c*). Moreover, a substantial proportion of HCC cells were immunostained with anti-Pim-3 IgY (6 of 27 cases; Fig. 5*d,e*) but not the pre-immunized IgY (data not shown). Furthermore, Pim-3 protein was observed markedly in regenerated proliferating bile ductules (27 of 27 cases; Fig. 5*c,f*, arrows). Because the staining patterns were similar to that observed in HBsTg mouse model (Fig. 2), these results would indicate that Pim-3 protein expression was aberrantly enhanced in precancerous lesion, also in humans, and a portion of HCC cells.

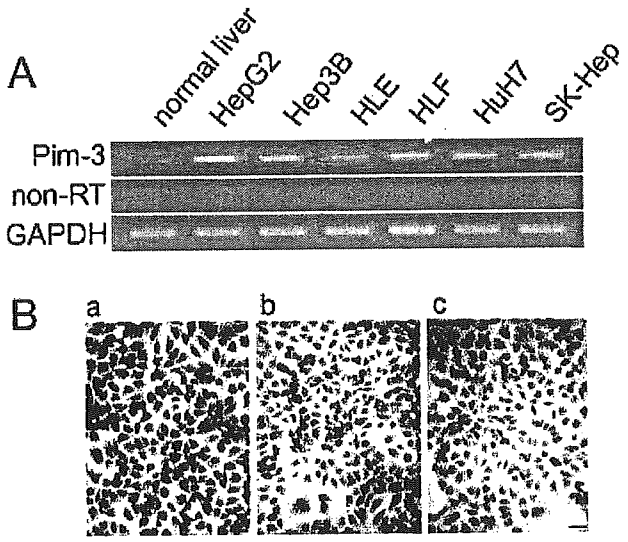

FIGURE 6 – (*a*) *Pim-3* mRNA expression in various human hepatoma cell lines. Total RNAs were extracted from human hepatoma cell lines and normal liver tissue. RT-PCR was carried out. Representative results from 3 independent experiments are shown here. Analysis for Pim-3 expression was carried out without reverse transcriptase treatment and the results are shown as non-RT. (*b*) Pim-3 protein expression in HuH7 cells. HuH7 cells were immunostained by anti-Pim-3 IgY (*b*[a]), by pre-immunized IgY (*b*[b]), or by anti-Pim-3 antibodies absorbed with the relevant peptide (*b*[c]) as described in Material and Methods. Representative results from 3 independent experiments are shown. Original magnification = ×400. Scale bars = 50 μm.

Constitutive Pim-3 expression in human hepatoma cell lines

Immunohistochemical analysis indicated that Pim-3 protein expression was aberrantly enhanced not only in precancerous lesion but also in a portion of HCC cells in human HCC tissues (Fig. 5). This finding prompted us to examine Pim-3 expression in human hepatoma cell lines, by RT-PCR. To exclude the possibility that contaminated genomic DNA gave rise to the generation of the amplified bands, we used total RNA samples that were treated with DNase. Under the present condition, *Pim-3* transcript was detected in all hepatoma cell lines, whereas no specific band was detected in the normal liver tissue (Fig. 6*a*), consistent with the Northern blotting analysis. The exclusion of reverse transcriptase failed to give rise to any bands, further indicating the specificities of RT-PCR (Fig. 6*a*; non-RT). Moreover, an immunocytochemical analysis detected immunoreactive Pim-3 proteins in HuH7 cell line, when incubated with anti-Pim-3 antibodies (Fig. 6*b*[a]) but neither pre-immunized IgY (Fig. 6*b*[b]) nor anti-Pim-3 adsorbed with the relevant peptide (Fig. 6*b*[c]). Immunoreactive Pim-3 proteins were similarly detected in all 6 human hepatoma cell lines, consistent with RT-PCR analysis (data not shown). Collectively, these results would indicate that Pim-3 was constitutively expressed in human hepatoma cell lines.

RNAi ablation of Pim-3 induces cell death to hepatoma cell lines

Because Pim-1 and Pim-2 were required to induce cell-cycle progression[21,22] and anti-apoptotic effects,[21–25] we examined the role of Pim-3 in cell proliferation by ablating endogenous *Pim-3* mRNA expression in HuH7 and Hep3B cell lines with RNAi. Endogenous *Pim-3* mRNA level was decreased after the transfection with specific *Pim-3* siRNA but not Scramble siRNA (Fig. 7*a*). Under these conditions, transfection with *Pim-3* siRNA significantly retarded cell proliferation, compared to Scramble siRNA-transfected and the control cells (Fig. 7*b,c*). These results sug-

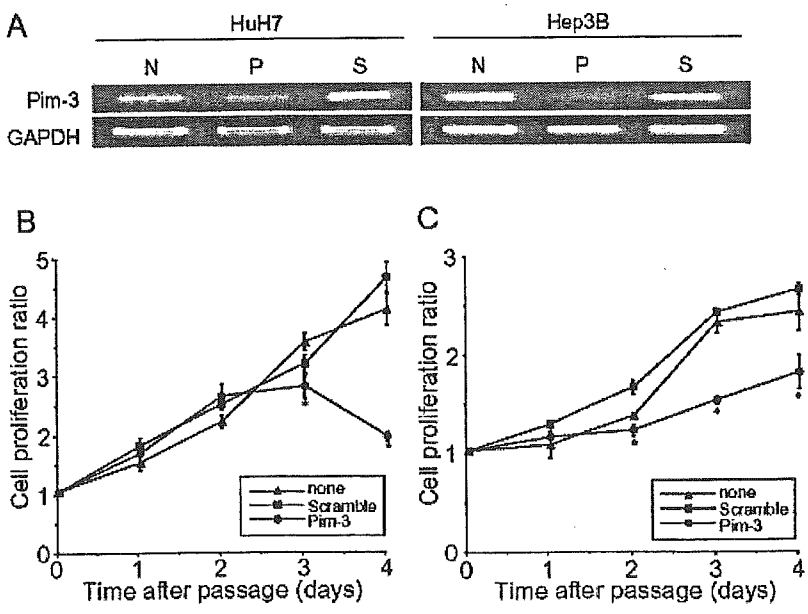

FIGURE 7 – The effects of endogenous Pim-3 ablation on cell proliferation. (*a*) Semi-quantitative RT-PCR analysis for *Pim-3* mRNA levels in siRNA transfected cells. Total RNAs were extracted from the transfectant with *Pim-3* siRNA (P), Scramble siRNA (S), or no siRNA (N) 2 (Hep3B) or 4 days (HuH7) after the transfection as described in Material and Methods. (*b,c*) Cell proliferation rates were determined on HuH7 (*b*) and Hep3B (*c*) cells transfected with *Pim-3* siRNA (◇), Scramble siRNA (□), or no siRNA (△) by WST-1 assay. Cells were trypsinized and 5×10^3 cells were plated to each well of 96-well plate at 2 days after the transfection. This time point was designated as Day 0. The ratios to Day 0 were calculated. Results are expressed as means ($n = 3$), and error bars indicate SD. Representative results from 3 independent experiments are shown. Statistical significance was evaluated using ANOVA test, and $p < 0.05$ was accepted as statistically significant. $^*p < 0.05$ compared to no siRNA samples at the same time point.

gested that Pim-3 ablation has adverse effects on the proliferation of hepatoma cell lines. We further observed that HuH7 cells detached from the plates later than 4 days after the transfection with *Pim-3* but not Scramble siRNA (Fig. 8*a*). Moreover, Pim-3 siRNA transfectants exhibited a higher ratio of sub-G1 populations with reduced G1 and G2/M populations, compared to Scramble siRNA transfectants and control cells (Fig. 8*b*). Furthermore, the proportion of cells with condensed nuclei was significantly higher in both HuH7 and Hep3B cells transfected with *Pim-3* siRNA, than those transfected with Scramble siRNA (Fig. 8*c*). These observations would indicate that the ablation of Pim-3 might induce apoptosis in these hepatoma cell lines.

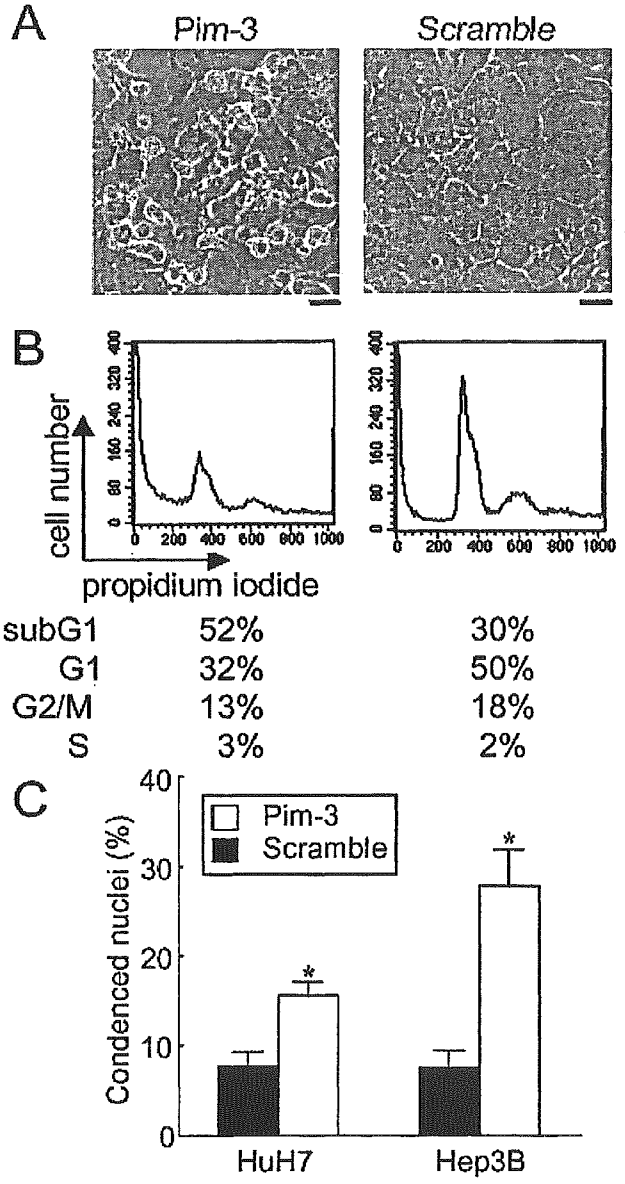

FIGURE 8 – The effects of endogenous Pim-3 ablation on apoptosis in HuH7 cells. (*a*) HuH7 cells were observed under an inverted microscope at 4 days after the transfection with *Pim-3* or Scramble siRNA under the same conditions as Figure 7. Representative results from 3 independent experiments are shown. Original magnification = ×200. Scale bars = 50 μm. (*b*) Cell-cycles were analyzed at 4 days after the transfection, by using a flow cytometry as described in Material and Methods. Representative results from 3 independent experiments are shown. (*c*) Chromatin condensation was analyzed at 4 days after the transfection as described in Material and Methods. Representative results from 3 independent experiments are shown. Results are expressed as means ($n = 6$), and bars indicate SE. Statistical significance was evaluated using ANOVA test and $p < 0.05$ was accepted as statistically significant. *$p < 0.05$ compared to Scramble siRNA samples.

Discussion

Transcriptome analysis has been applied widely to elucidate molecular mechanisms of various types of diseases and can provide many important clues, particularly for understanding the molecular pathogenesis of oncogenesis, where the expression of many genes changes simultaneously.[26,27] Several independent groups carried out transcriptomal studies on human HCC.[28–33] In most studies, however, the gene expression pattern was compared between tumor and non-tumor portions obtained from the same patients.[28–33] Because these non-tumor portions exhibit usually hepatocyte dysplasia, this type of analysis may fail to detect the changes in gene expression that have already existed at the stage of hepatocyte dysplasia. To circumvent these pitfalls, we compared gene expression patterns between pre-malignant lesions and normal tissues by using FDD. We observed that various genes were selectively changed in pre-malignant lesions. Moreover, a semi-quantitative RT-PCR analysis did not detect any significant differences in the expression of several of these genes between malignant and pre-malignant lesions (our unpublished data), supporting our assumption that the changes in gene expression which have already existed at the stage of hepatocyte dysplasia, might be undetected in the preceding studies.

Among the genes identified in our study, we focused on Pim-3. Pim-3 was originally identified as depolarization-induced gene KID-1 in PC12 cell line, a rat pheochromocytoma cell line.[8] Subsequently, several independent groups observed a selective expression of its mRNA in neuronal system,[16,34,35] but not the liver. By using human *Pim-3* cDNA as a probe, we detected *Pim-3* mRNA in several organs such as the brain and spleen but not the liver. On the contrary, *Pim-3* mRNA expression was detected in all human hepatoma cell lines that we examined. Moreover, immunohistochemical analysis detected immunoreactive Pim-3 protein in precancerous lesions and a portion of HCC cells. Furthermore, Pim-3 protein was also detected in regenerating bile ductules, which are assumed to be the proliferation of hepatic stem cells after chronic liver injury (*i.e.*, infection, tumors).[14]

Deneen *et al.*[36] provided evidence on the crucial involvement of Pim-3 in EWS/ETS-mediated malignant transformation of mouse NIH 3T3 cells. They demonstrated that Pim-3 was a common transcriptional target of EWS/ETS. EWS/ETS fusion proteins retain an intact ETS DNA-binding domain and can bind to a binding sequence in the target genes through this domain.[37] *Pim-3* gene transcription may be regulated not only by EWS/ETS fusion proteins but also other Ets family proteins. Several independent groups reported that Ets-1, one of the Ets family proteins, was expressed in human HCC tissues.[38,39] Ito *et al.*[38] demonstrated that Ets-1 expression was markedly enhanced in non-cancerous lesions adjacent to HCC lesions and suggested that Ets-1 had a crucial role in hepatocarcinogenesis and HCC progression during their early phases. In line with these observations, we also observed that another transcription factor with an ETS-domain, polyomavirus enhancer A binding protein-3, was expressed selectively in HCC and induced constitutive gene expression of a pro-angiogenic factor, interleukin (IL)-8, in HCC.[40] It is tempting to speculate that a transcription factor(s) with an ETS-domain, may induce ectopic Pim-3 gene expression in liver, during the course of hepatocarcinogenesis.

Several lines of evidence demonstrated that the gene expression of *Pim-1* and *Pim-2* could be regulated by IL-6-gp130-mediated signal transducers and activators of transcription (STAT) family

protein, STAT3.[41,42] STAT3 signals can advance cell-cycles and prevent apoptosis by inducing Pim-1 and c-Myc in lymphomagenesis.[42] In the liver, IL-6-deficient mice exhibited an impaired liver regeneration after a partial hepatectomy.[43] Several lines of evidence have shown that Bcl-xL expression is upregulated by IL-6-gp130-mediated STAT3 and prevents hepatocyte apoptosis,[45,46] and the constitutive activation of STATs observed during oncogenesis can cause a permanent alteration in the genetic program.[45,46] These observations suggest that STAT3 signals could regulate hepatocyte regeneration during the course of HBV-induced hepatocarcinogenesis. We observed that *Pim-3* gene ablation by RNAi attenuated proliferation rates and caused cell death in hepatoma cell lines. Thus, if Pim-3 was also regulated by STAT3, these observations suggest that Pim-3 would be involved in STAT3-mediated prevention of apoptosis or cell-cycle progression.

Pim-1 and Pim-2 are also known as proto-oncogene to be involved in lymphomagenesis.[47,48] Because Pim-1 and Pim-2 can induce anti-apoptotic effects,[21–25] Pim-3 may be involved in cell-cycle regulation or anti-apoptosis. We also observed that gene ablation of Pim-3 caused cell death to human hepatoma cell lines, later than 3 days after the transfection. These results suggest that Pim-3 can regulate cell-cycle or apoptosis process indirectly by phosphorylating a molecule(s) upstream in these processes. Although Pim-1 can phosphorylate several molecules such as Cdc25A,[49] a G_1/S cell-cycle regulator, Pim-3 could not interact with Cdc25A.[36] Pim-1 can also phosphorylate valosine containing protein (VCP)/p97,[41,42] a mammalian homolog of *Saccaromyces cerevisiae* Cdc48p. Pim-1 can upregulate further the expression of an anti-apoptotic molecule, Bcl-2 and Bcl-xL, by augmenting the expression of VCP.[42,43] In HCC tissues and human hepatoma cell lines, evidence is accumulating to indicate that Bcl-xL is constitutively expressed and is a major executer to prevent apoptosis.[50–52] Moreover, VCP was also detected in human HCC tissues.[53] If VCP could be phosphorylated by Pim-3 as well as Pim-1, Pim-3 may exert an anti-apoptosis effect by augmenting indirectly the expression of an anti-apoptotic molecule, similarly as Pim-1. Moreover, if the contents of target molecules may differ between HuH7 and Hep3B cell lines, these may account for different patterns of the effects of Pim-3 gene ablation on the proliferation of these cell lines.

The kinase activity of Pim-3 was crucially involved in EWS/ETS-mediated malignant transformation of mouse NIH 3T3 cells.[36] Our present observations suggest that Pim-3 can regulate anti-apoptosis process or cell-cycle progression by modulating molecules involved in these processes. Accumulating evidence indicated that Pim-3 can auto-phosphorylate itself,[8,17] but it still remains elusive on physiological substrates of Pim-3. The identification of a substrate(s) may shed novel light on Pim-3-mediated regulatory mechanisms of apoptosis or cell-cycle progression.

References

1. Schafer DF, Sorrell MF. Hepatocellular carcinoma. Lancet 1999;353:1253–7.
2. Geller SA. Hepatitis B and hepatitis C. Clin Liver Dis 2002;6:317–34.
3. Iino S. Natural history of hepatitis B and C virus infections. Oncology 2002;62:18–23.
4. Bertoletti A, Maini MK. Protection or damage: a dual role for the virus-specific cytotoxic T lymphocyte response in hepatitis B and C infection? Curr Opin Immunol 2000;12:403–8.
5. Hino O, Kajino K, Umeda T, Arakawa Y. Understanding the hypercarcinogenic state in chronic hepatitis: a clue to the prevention of human hepatocellular carcinoma. J Gastroenterol 2002;37:883–7.
6. Nakamoto Y, Guidotti LG, Kuhlen CV, Fowler P, Chisari FV. Immune pathogenesis of hepatocellular carcinoma. J Exp Med 1998;188:341–50.
7. Nakamoto Y, Suda T, Momoi T, Kaneko S. Different procarcinogenic potentials of lymphocyte subsets in a transgenic mouse model of chronic hepatitis B. Cancer Res 2004;64:3326–33.
8. Feldman JD, Vician L, Crispino M, Tocco G, Marcheselli VL, Bazan NG, Baudry M, Herschman HR. KID-1, a protein kinase induced by depolarization in brain. J Biol Chem 1998;273:16535–43.
9. Chisari FV, Filippi P, McLachlan A, Milich DR, Riggs M, Lee S, Palmiter RD, Pinkert CA, Brinster RL. Expression of hepatitis B virus large envelope polypeptide inhibits hepatitis B surface antigen secretion in transgenic mice. J Virol 1986;60:880–7.
10. Wirth S, Guidotti LG, Ando K, Schlicht HJ, Chisari FV. Breaking tolerance leads to autoantibody production but not autoimmune liver disease in hepatitis B virus envelope transgenic mice. J Immunol 1995;154:2504–15.
11. Ito T, Sakaki Y. Fluorescent differential display: a fast and reliable method for message display polymerase chain reaction. Methods Enzymol 1999;303:298–309.
12. Lu P, Nakamoto Y, Nemoto-Sasaki Y, Fujii C, Wang H, Hashii M, Ohmoto Y, Kaneko S, Kobayashi K, Mukaida N. Potential interaction between CCR1 and its ligand, CCL3, induced by endogenously produced interleukin-1 in human hepatomas. Am J Pathol 2003;162:1249–58.
13. Kitamura K, Nakamoto Y, Akiyama M, Fujii C, Kondo T, Kobayashi K, Kaneko S, Mukaida N. Pathogenic roles of tumor necrosis factor receptor p55-mediated signals in dimethylnitrosamine-induced murine liver fibrosis. Lab Invest 2002;82:571–83.
14. Wang X, Foster M, Al-Dhalimy M, Lagasse E, Finegold M, Grompe M. The origin and repopulating capacity of murine oval cells. Proc Natl Acad Sci USA 2003;100:11881–8.
15. Mikkers H, Allen J, Knipscheer P, Romeyn L, Hart A, Vink E, Berns A. High-throughput retroviral tagging to identify components of specific signaling pathways in cancer. Nat Genet 2002;32:153–9.
16. Konietzko U, Kauselmann G, Scafidi U, Staubli U, Mikkers H, Berns A, Schweizer M, Waltereit R, Kuhl D. Pim kinase expression is induced by LTP stimulation and required for the consolidation of enduring LTP. EMBO J 1999;18:3359–69.
17. Eichmann A, Yuan L, Bréant C, Alitalo K, Koskinen PJ. Developmental expression of Pim kinases suggests functions also outside of the hematopoietic system. Oncogene 2000;19:1215–24.
18. Palaty CK, Kalmar G, Tai G, Oh S, Amankawa L, Affolter M, Aebersold R, Pelech SL. Identification of the autophosphorylation sites of the *Xenopus laevis* Pim-1 proto-oncogene-encoded protein kinase. J Biol Chem 1997;272:10514–21.
19. Houri RZ, Hazum S, Givol D, Telerman A. The cDNA sequence and gene analysis of the human *pim* oncogene. Gene 1987;54:105–11.
20. Baytel D, Shalom S, Madger I, Weissenberg R, Don J. The human *Pim-2* proto-oncogene and its testicular expression. Biochim Biophys Acta 1998;1442:274–85.
21. Möröy T, Grzeschiczek A, Petzold S, Hartmann KU. Expression of a *Pim-1* transgene accelerates lymphoproliferation and inhibits apoptosis in *lpr/lpr* mice. Proc Natl Acad Sci USA 1993;90:10734–8.
22. Wang Z, Bhattacharya N, Weaver M, Petersen K, Meyer M, Gapter L, Magnuson NS. Pim-1: a serine/threonine kinase with a role in cell survival, proliferation, differentiation and tumorigenesis. J Vet Sci 2001;2:167–79.
23. Skorska MN, Hoser G, Kossev P, Wasik MA, Skorski T. Complementary functions of the antiapoptotic protein A1 and serine/threonine kinase pim-1 in the BCR/ABL-mediated leukemogenesis. Blood 2002;99:4531–9.
24. Fox CJ, Hammerman PS, Cinalli RM, Master SR, Chodosh LA, Thompson CB. The serine/threonine kinase Pim-2 is a transcriptionally regulated apoptotic inhibitor. Genes Dev 2003;17:1841–54.
25. Yan B, Zemskova M, Holder S, Chin V, Kraft A, Koskinen PJ, Lilly M. The PIM-2 kinase phosphorylates BAD on serine 112 and reverses BAD-induced cell death. J Biol Chem 2003;278:45358–67.
26. Liotta L, Petricoin E. Molecular profiling of human cancer. Nat Rev Genet 2000;1:48–56.
27. Thorgeirsson SS, Grisham JW. Molecular pathogenesis of human hepatocellular carcinoma. Nat Genet 2002;31:339–46.
28. Honda M, Kaneko S, Kawai H, Shirota Y, Kobayashi K. Differential gene expression between chronic hepatitis B and C hepatic lesion. Gastroenterology 2001;120:955–66.
29. Kim MY, Park E, Park JH, Park DH, Moon WS, Cho BH, Shin HS, Kim DG. Expression profile of nine novel genes differentially expressed in hepatitis B virus-associated hepatocellular carcinomas. Oncogene 2001;20:4568–75.
30. Shirota Y, Kaneko S, Honda M, Kawai HF, Kobayashi K. Identification of differentially expressed genes in hepatocellular carcinoma with cDNA microarrays. Hepatology 2001;33:832–40.
31. Smith MW, Yue ZN, Geiss GK, Sadovnikova NY, Carter VS, Boix L, Lazaro CA, Rosenberg GB, Bumgarner RE, Fausto N, Bruix J, Katze MG. Identification of novel tumor markers in hepatitis C virus-associated hepatocellular carcinoma. Cancer Res 2003;63:859–64.
32. Xu XR, Huang J, Xu ZG, Qian BZ, Zhu ZD, Yan Q, Cai T, Zhang X,

Xiao HS, Qu J, Liu F, Huang QH, et al. Insight into hepatocellular carcinogenesis at transcriptome level by comparing gene expression profiles of hepatocellular carcinoma with those of corresponding noncancerous liver. Proc Natl Acad Sci USA 2001;98:15089–94.
33. Yamashita T, Kaneko S, Hashimoto S, Sato T, Nagai S, Toyoda N, Suzuki T, Kobayashi K, Matsushima K. Serial analysis of gene expression in chronic hepatitis C and hepatocellular carcinoma. Biochem Biophys Res Commun 2001;282:647–54.
34. Giza CC, Prins ML, Hovda DA, Herschman HR, Feldman JD. Genes preferentially induced by depolarization after concussive brain injury: effects of age and injury severity. J Neurotrauma 2002;19:387–402.
35. Lu A, Tang Y, Ran R, Clark JF, Aronow BJ, Sharp FR. Genomics of the periinfarction cortex after focal cerebral ischemia. J Cereb Blood Flow Metab 2003;23:786–810.
36. Deneen B, Welford SM, Ho T, Hernandez F, Kurland I, Denny CT. PIM3 proto-oncogene kinase is a common transcriptional target of divergent EWS/ETS oncoproteins. Mol Cell Biol 2003;23:3897–908.
37. Arvand A, Denny CT. Biology of EWS/ETS fusions in Ewing's family tumors. Oncogene 2001;20:5747–54.
38. Ito Y, Miyoshi E, Takeda T, Sakon M, Noda K, Tsujimoto M, Monden M, Taniguchi N, Matsuura N. Expression and possible role of *ets*-1 in hepatocellular carcinoma. Am J Clin Pathol 2000;114:719–25.
39. Kanda K, Nakayama T, Onizuka S, Tomioka T, Kanematsu T. Expression of the Ets-1 proto-oncogene is linked to cell differentiation of human hepatocellular carcinoma. Hepatogastroenterology 2002;49:746–51.
40. Iguchi A, Kitajima I, Yamakuchi M, Ueno S, Aikou T, Kubo T, Matsushima K, Mukaida N, Maruyama I. PEA3 and AP-1 are required for constitutive IL-8 gene expression in hepatoma cells. Biochem Biophys Res Commun 2000;279:166–71.
41. Hirano T, Ishihara K, Hibi M. Roles of STAT3 in mediating the cell growth, differentiation and survival signals relayed through the IL-6 family of cytokine receptors. Oncogene 2000;19:2548–56.
42. Shirogane T, Fukada T, Muller JMM, Shima DT, Hibi M, Hirano T. Synergistic roles for Pim-1 and c-Myc in STAT3-mediated cell-cycle progression and anti-apoptosis. Immunity 1999;11:709–19.
43. Cressman DE, Greenbaum LE, DeAngelis RA, Ciliberto G, Furth EE, Poli V, Taub R. Liver failure and defective hepatocyte regeneration in interleukin-6-deficient mice. Science 1996;274:1379–83.
44. Wuestefeld T, Klein C, Streetz KL, Betz U, Lauber J, Buer J, Manns MP, Müller W, Trautwein C. Interleukin-6/glycoprotein 130-dependent pathways are protective during liver regeneration. J Biol Chem 2003;278:11281–8.
45. Bowman T, Garcia R, Turkson J, Jove R. STATs in oncogenesis. Oncogene 2000;19:2474–88.
46. Bromberg J. Stat proteins and oncogenesis. J Clin Invest 2002;109:1139–42.
47. van Lohuizen M, Verbeek S, Krimpenfort P, Domen J, Saris C, Radaszkiewicz T, Berns A. Predisposition to lymphomagenesis in *pim-1* transgenic mice: cooperation with *c-myc* and *N-myc* in murine leukemia virus-induced tumors. Cell 1989;56:673–82.
48. Allen JD, Verhoeven E, Domen J, van der Valk M, Berns A. *Pim-2* transgene induces lymphoid tumors, exhibiting potent synergy with *c-myc*. Oncogene 1997;15:1133–41.
49. Takehara T, Liu X, Fujimoto J, Friedman SL, Takahashi H. Expression and role of Bcl-xL in human hepatocellular carcinomas. Hepatology 2001;34:55–61.
50. Mochizuki T, Kitanaka C, Noguchi K, Muramatsu T, Asai A, Kuchino Y. Physical and functional interactions between Pim-1 kinase and Cdc25A phosphatase. J Biol Chem 1999;274:18659–66.
51. Pierce RH, Vail ME, Ralph L, Campbell JS, Fausto N. Bcl-2 expression inhibits liver carcinogenesis and delays the development of proliferating foci. Am J Pathol 2002;160:1555–60.
52. Watanabe J, Kushihata F, Honda K, Mominoki K, Matsuda S, Kobayashi N. Bcl-xL overexpression in human hepatocellular carcinoma. Int J Oncol 2002;21:515–19.
53. Yamamoto S, Tomita Y, Nakamori S, Hoshida Y, Nagano H, Dono K, Umeshita K, Sakon M, Monden M, Aozasa K. Elevated expression of valosin-containing protein (p97) in hepatocellular carcinoma is correlated with increased incidence of tumor recurrence. J Clin Oncol 2003;21:447–52.

La Protein Is a Potent Regulator of Replication of Hepatitis C Virus in Patients With Chronic Hepatitis C Through Internal Ribosomal Entry Site–Directed Translation

MASAO HONDA, TAKEO SHIMAZAKI, and SHUICHI KANEKO
Department of Gastroenterology, Kanazawa University Graduate School of Medicine, Kanazawa, Japan

Background & Aims: Translation of hepatitis C virus is an essential step of viral replication and is mediated by an internal ribosome entry site. We previously reported that the hepatitis C virus internal ribosome entry site is most active during the synthetic (S) or mitotic (M) phases and lowest during quiescent (G_0) phase. Here, we investigated host factors responsible for the regulation of the hepatitis C virus internal ribosome entry site. *Methods:* We synchronized the cell-cycle progression and evaluated gene-expression dynamics of host factors and kinetics of hepatitis C virus internal ribosome entry site activity in cells at various points during the cell cycle by using a complementary DNA microarray. We also validated the significance of identified host factors on hepatitis C virus replication in vivo. *Results:* Hepatitis C virus internal ribosome entry site activity correlated with a gene cluster induced in the S and G_2/M phases. It is interesting to note that most initiation factors known to bind or interact with the hepatitis C virus internal ribosome entry site [poly(rC)-binding protein 2, polypyrimidine tract binding protein, eukaryotic initiation factor 3, eukaryotic initiation factor 2γ, eukaryotic initiation factor 2β, La protein, and heterogenous nuclear ribonucleoprotein L] were induced during the S and G_2/M phases. Expression of La protein, polypyrimidine tract binding protein, and eukaryotic initiation factor 3 (p116, p170) were predominantly repressed in G_0 phase and induced in S and G_2/M phases. Suppression or overexpression of La protein and polypyrimidine tract binding protein in RCF-26 significantly changed hepatitis C virus internal ribosome entry site activity. In the livers of patients with chronic hepatitis C, expression of La protein was significantly increased and correlated with the amount of hepatitis C virus RNA. *Conclusions:* Hepatitis C virus uses host factors induced during cell division but not during quiescence for replication. Of these, La protein is a potent regulator and enhances hepatitis C virus replication in regenerating hepatocytes in patients with chronic hepatitis C.

Hepatitis C virus (HCV), a positive-strand enveloped RNA virus, belongs to the genus *Hepacivirus* of the family Flaviviridae.[1] The human liver infected with HCV develops chronic hepatitis, cirrhosis, and, in some instances, hepatocellular carcinoma.[1,2] Although a combination of ribavirin and interferon has become a popular means of treating infected patients, the results are often unsatisfactory, especially in patients with a high viral load.[3–6] Identification of host factors that regulate HCV replication in infected patients could be helpful in the development of a novel antiviral treatment strategy.

Translation of the polyproteins of the HCV RNA genome is an essential step in viral replication and is supposed to be a fruitful target of new antiviral treatment strategies, such as antisense oligonucleotide (oligo) or small interference RNA. Translation of HCV is initiated by a highly structured RNA segment, the internal ribosome entry site (IRES), that occupies most of the 5′-nontranslated (5′-NTR) RNA.[7–15] The translation machinery of HCV is simple and, because it is a prokaryote, requires only the ribosomal 40S subunit, the eukaryotic initiation factor (eIF)2/guanosine triphosphate/Met-transfer RNA complex, and eIF3 to initiate translation.[7] In contrast, cap-dependent translation is more complex and requires additional canonical initiation factors, such as eIF4E, eIF4G, eIF4A, and eIF4B.[7] Many other noncanonical translation initiation factors, such as La protein,[16,17] polypyrimidine tract binding protein (PTB),[18] heterogeneous nuclear ribonucleoprotein L (RNPL),[19] poly(rC)-binding protein (PCBP)-2,[20] and ribosomal protein S9,[7] interact with HCV IRES and might regulate HCV translation. Thus, the machineries of cap-dependent and HCV IRES–directed translation

Abbreviations used in this paper: CMV, cytomegalovirus; eIF, eukaryotic initiation factor; FBS, fetal bovine serum; FL, firefly luciferase; IRES, internal ribosome entry site; nt, nucleotide; 5′-NTR, 5′ nontranslated region; oligo, oligonucleotide; PABPC, poly(A)-binding protein, cytoplasmic; PCBP, poly(rC)-binding protein; PTB, polypyrimidine tract binding protein; RL, *Renilla* luciferase; RNPL, heterogeneous nuclear ribonucleoprotein L; RTD, real-time detection; RT-PCR, reverse-transcription polymerase chain reaction; SOM, self-organizing map.

0016-5085/05/$30.00
doi:10.1053/j.gastro.2004.11.064

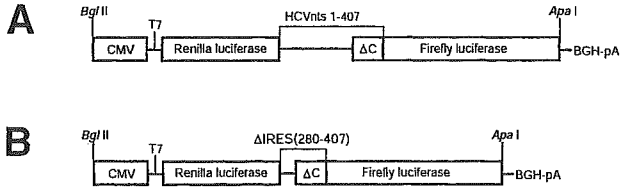

Figure 1. Organization of the transcriptional unit of plasmid pRL-HL and pRL-(ΔIRES)-HL. (*A*) Plasmid pRL-HL[22] contains a dicistronic CMV transcriptional cassette in which upstream *Renilla* and downstream firefly luciferase genes are separated by the complete 5′-NTR and 66-nt core sequence of HCV (nts 1–407; strain 1b) placed in the intercistronic space. (*B*) Plasmid pRL-(ΔIRES)-HL was the control plasmid of pRL-HL in which the functional HCV IRES element (nts 1–279) was deleted. CMV, cytomegalovirus promoter; T7, Bacteriophage T7 RNA polymerase promoter; BGH-pA, bovine growth hormone polyadenylation signal.

can be differentiated in terms of requirements for canonical and noncanonical initiation factors.[21]

We previously found that HCV IRES activity varies during the cell cycle and is greatest during the synthetic (S) or mitotic (M) phases and lowest during the quiescent (G_0) phase.[22] These findings suggest that HCV translation is regulated by cellular proteins that vary in abundance during the cell cycle and that viral replication is enhanced by factors that stimulate the regeneration of hepatocytes in patients with chronic hepatitis C. This finding implies that inflammation and the resulting increased turnover in hepatocytes may increase the number of actively dividing hepatocytes, resulting in increased IRES activity and enhanced HCV replication.

This study profiles the expression of cellular proteins during cell-cycle progression and identifies factors responsible for cell cycle–dependent HCV IRES–directed translation. We evaluated whether those factors are in fact related to HCV replication in the livers of patients with chronic hepatitis C.

Materials and Methods

Plasmids

Plasmid pRL-HL contains a dicistronic cytomegalovirus (CMV) transcriptional cassette in which an upstream *Renilla* luciferase (RL) gene and a downstream firefly luciferase (FL) gene are separated by the complete 5′-NTR and 66-nucleotide (nt) core sequence of HCV (nts 1–407 of a genotype 1b strain) placed within the intercistronic space[22] (Figure 1*A*). Plasmid pRL-(ΔIRES)-HL was the control plasmid of pRL-HL in which the functional HCV IRES element (nts 1–279) had been deleted (Figure 1*B*). This plasmid was constructed by subcloning the 1.82-kilobase *StuI*/*ApaI* fragment of pRL-HL (containing the deleted HCV IRES element [nts 280–341 of the HCV-1b 5′-NTR sequence and 66 nts of the core sequence] fused directly to FL) into the multiple cloning site of pBluescript IISK (Stratagene, La Jolla, CA). A 1.82-kilobase *NotI*/*ApaI* fragment was subsequently excised from this plasmid and cloned into the *NotI*/*ApaI* site of pRL-HL.

The La expression vector pCMV-La was constructed as previously described.[23] The PTB expression vector pRC/CMV-PTB, the RNPL expression vector pcDNA3-myc-hnRNPL, and the PCBP-1 and PCBP-2 expression vectors pcDNA3-myc-haCP1 and pcDNA3-myc-haCP2 were provided by Dr. Stanley M. Lemon,[24] Dr. Gideon Dreyfuss,[25] and Dr. Stephen A. Liebhaber,[26] respectively. Dr. John W. B. Hershey provided the eIF2γ full-length clone in pSP72.[27] We constructed the eIF2γ expression vector pCMV-eIF2-γ by excising the *Eco*RI and *Eco*RI fragment of full-length coding sequences and cloning into *Eco*RI of pCR 3.1 (Invitrogen, San Diego, CA) under the control of the CMV promoter. Dr. Keith Johnson provided the eIF3 p170 full-length clone in PUC19.[28] We constructed the eIF3 p170 expression vector pCMV-eIF3 p170 by excising the *Kpn*I and *Sna*BI fragment of full-length coding sequences and cloning into *Kpn*I and *Eco*RV of pCR 3.1 under the control of the CMV promoter. The complementary DNA (cDNA) of ribosomal protein S9 was cloned by reverse-transcription polymerase chain reaction (RT-PCR) of total RNA isolated from Huh-7 cells by using sense (5′-ACGGTGGAAGCGGACG-CAACATGCCAGTGG-3′) and antisense (5′-GGGACAG-GTGGACTTAATCCTCCTCCTCGTCG-3′) primers. The resultant cDNA was cloned into the TOPO TA cloning vector (Invitrogen), and nt sequences were confirmed. The expression vector pCMV-S9 was constructed by excising and cloning *Hin*dIII and *Xho*I fragments from TOPO TA into the same sites of pCR 3.1.

Cell Lines

The RCF-26 was a stably transformed cell line from Huh-7 cells (human hepatocellular carcinoma cells) that constitutively express dicistronic RNA transcripts containing sequences encoding 2 reporter proteins, RL and FL, separated by a functional HCV IRES[22] (Figure 1*A*). The ΔRCF-9 was a stably transformed cell line from Huh-7 cells that constitutively expressed dicistronic RNA transcripts in which the functional HCV IRES element (nts 1–279) had been deleted (Figure 1*B*).

Overexpression of Canonical and Noncanonical Initiation Factors in RCF-26

The RCF-26 cells were cultured in Dulbecco's modified Eagle medium (Gibco BRL, Gaithersburg, MD) containing 10% fetal bovine serum (FBS), 1% penicillin/streptomycin, and 400 μg/mL of Geneticin (active compound) (Gibco BRL, Gaithersburg, MD). Cells cultured in a 5% CO_2 incubator at 37°C were transfected with 0.5–1.0 μg of plasmid DNA by using FuGENE 6 (Roche Molecular Biochemicals, Basel, Switzerland) according to the manufacturer's instructions. After 24–48 hours of transfection, the cells were harvested, and reporter genes were assayed.

Reporter Gene Assays

Cells cultured in 10- or 15-cm dishes in Dulbecco's modified Eagle medium containing 10% FBS were trypsinized. A quarter of the cells were lysed in 1 mL of passive lysis buffer (25 mmol/L Tris-phosphate [pH 7.8], 2 mmol/L dithiothreitol, 2 mmol/L 1,2-diaminocyclohexane-N,N,N′,N′-tetraacetic acid, 10% glycerol, and 1% Triton X-100). RL and FL activities were measured in 20 μL of cell lysate by using the Dual-Luciferase Reporter Assay System (Promega, Madison, WI). Total RNA was isolated from the remainder and processed for analysis by cDNA microarray, Northern blotting, and real-time detection (RTD) PCR.

Antisense Oligodeoxynucleotide

We designed respective antisense phosphorothioate oligos that were complementary to the sequence from 5 nts upstream to 15 downstream of the predicted translational initiation site of the La protein, PTB, eIF3 p170, eIF2γ, RNPL, poly(A)-binding protein, cytoplasmic 1 (PABPC-1), PCBP-2, and ribosomal protein S9 gene. The nt sequences of antisense oligos were 5′-GCCATTACGGCTATCTTTAA-3′ for La protein, 5′-TCCATGGCACACAGAGCAGA-3′ for PTB, 5′-GGCATTTTCCGGCCTCTGAA-3′ for eIF3 p170, 5′-CCAGCTTCTCCGCCCGCCAT-3′ for eIF2γ, 5′-ACCATCGCTCCCGACCGCCT-3′ for RNPL, 5′-TTCATCTCGGCACGGCTGCC-3′ for PABPC-1, 5′-TCCATGTCGAGCAGTGTTCT-3′ for PCBP-2, and 5′-GGCATGTTGCGTCCGCTTCCGCC-3′ for ribosomal protein S9. Positive and negative controls consisted of an antisense oligo for the 5′ region of HCV (nt 330–350), 5′-GTGCTCATGGTGCACGGTCT-3′,[29] and the randomized oligo, 6961, 5′-TACGTTTCTATGTCGATGGG-3′,[29] respectively. Oligodeoxynucleotides (0.5–1.0 μmol/L) were added to the medium by using the FuGENE6 transfection reagent (Boehringer Mannheim, Mannheim, Germany), and the cultures were incubated for 24 hours. Cells were harvested, and HCV IRES activity was evaluated by assaying the reporter genes. To validate repressed targeted gene expression, 1 μg of total RNA was amplified by RT-PCR with specific primers for La protein, PTB, eIF3 p170, and ribosomal protein S9. The internal control was the level of β-actin expression.

Synchronization of Cell Growth and Analysis of Cellular DNA Content

To examine the relationship between HCV IRES–directed translation and cell growth, RCF-26 cells and ΔRCF-9 cells were incubated in 15-cm dishes with low serum or at confluence for 24–48 hours. RCF-26 cells and ΔRCF-9 cells in 10-cm dishes were synchronized at the G_1/S phase border by starvation for 24 hours in medium containing 0.1% FBS, followed by a wash and an 18-hour incubation in medium containing 10% FBS and 2.5 μg/mL aphidicolin. Aphidicolin was removed from the synchronized cells by washing and adding fresh medium containing 1% FBS. The cells were harvested at 3-hour intervals over 48 hours to assess the cell-cycle phase and reporter enzyme activities. The cell-cycle phase distribution in each sample cell population was determined by measuring the DNA content of individual cells by flow cytometry.[22]

Complementary DNA Microarray Analysis

We profiled gene expression in cells at different phases of the cell cycle by cDNA microarray analysis. We reconstructed the gene set of cDNA microarray slides containing 1080 cDNA clones[30] by adding canonical and noncanonical initiation factors. The new microarray included La protein,[16] PTB,[18] eIF2β,[31] eIF2γ,[31] eIF3 p116, eIF3 p170,[32] RNPL,[19] ribosomal protein S9,[7] PCBP-2,[20] PABPC-1,[33] and cell division cycle 2–like 1 (PITSLRE proteins)[34] that bind HCV or other viral IRES structures and might affect the IRES activity. Other canonical initiation factors, such as eIF1A, eIF2A, eIF4A, eIF4B, eIF4E, and eIF5,[7,21,35] were also included to analyze cap-dependent translation machinery.

Total RNA (50 μg) isolated from serum-starved or confluent cells (10% FBS and at 60%–70% cell density) was labeled with a fluorescent dye for the cDNA microarray.[30,36,37] To profile gene expression in cells during the cell cycle, total RNA was periodically extracted from synchronized cells at 3, 9, 15, 18, 24, 30, 36, and 42 hours released from aphidicolin block (G_1/S border). After 1 round of amplification, antisense RNA was labeled and hybridized with the cDNA microarray.[30,36,37] Images were acquired, and cDNA microarray slides were analyzed as previously described.[30,36,37] A 1-dimensional self-organizing map (SOM) was constructed to cluster genes with a similar expression profile throughout cell-cycle progression (Cluster and Tree view; http://www.microarrays.org.html/software).

Northern Blotting

We evaluated La protein, PTB, and albumin expression in cultured cells and in tissue samples by Northern blotting. Total RNA (20 μg) was separated on denaturing agarose/formaldehyde gels, transferred to a membrane, and hybridized with specific probes under standard conditions.

Western Blotting

RCF-26 cells seeded in a 10-cm dish were grown to subconfluency and washed twice with phosphate-buffered saline. Cells were lysed in radioimmunoprecipitation assay buffer. Cell lysates were collected by pelleting cell debris, and the concentration of protein was quantified by using a dye-binding assay (Bio-Rad, Hercules, CA). Eighty micrograms of cell lysate was electrophoresed in a sodium dodecyl sulfate/12.5% polyacrylamide gel and electrotransferred to a nitrocellulose membrane. After blocking with phosphate-buffered saline with 0.3% Tween-20 containing 5% skim milk for 1 hour, the membranes were reacted with appropriate antibodies. After washing with phosphate-buffered saline with 0.3% Tween-20, membranes were reacted with horseradish peroxidase–conjugated anti-mouse immunoglobulin G or anti-rab-

bit immunoglobulin G antibodies diluted 1:3000. Membranes were washed again and then visualized with an enhanced chemiluminescence kit (Amersham Pharmacia Biotech, Uppsala, Sweden).

Real-Time Detection Polymerase Chain Reaction

The PCR reaction mixture was prepared by using TaqMan Universal Master Mix (PE Applied Biosystems, Foster City, CA). The primer set applied to amplify La protein messenger RNA (mRNA) consisted of 5′-CGCTGGGAGGTGGAGTCGTT-3′ (exon 1) and 5′-CCCGTGGCAAATTGAAGTCG-3′ (exon 2). The probe, 5′-TGCCCTGGAGGCCAAAATCTGTCATC-3′ (exon 2), was designed to target an internal region between the forward and reverse primers. The primer set for PTB mRNA was 5′-AGCACGCCAAGCTGTCGCT-3′ (exon 8) and 5′-GGAACGGAAAGGCCGAAGG-3′ (exons 8–10). The probe was 5′-ACACACGCCCAGACCTGCCTTCCG-3′ (exon 8). The primer set for eIF3 p170 protein mRNA was 5′-CCGGAAAATGCCCTCAAACTA-3′ (exon 1) and 5′-AAGTGGCTCTTGCGAAGATCCACGC-3′ (exon 7). The probe sequence was 5′-CCAACGAATTTCTTGAGGTT-3′ (exon 2). The primer set for the internal control glyceraldehyde-3-phosphate dehydrogenase mRNA was designed according to GenBank M33197 by using the following primers: exon 7, 5′-TGCACCACCAACTGCTTAGCACCC-3′; and exon 8, 5′-CTTGATGTCATCATATTTGGCAGG-3′. The probe for glyceraldehyde-3-phosphate dehydrogenase-P, designed on the basis of exons 7 and 8, was 5′-TGACCACAGTCCATGCCATCACTGC-3′. Fifty PCR amplification cycles of 95°C for 30 seconds, 60°C for 40 seconds, and 72°C for 30 seconds were repeated by using a real-time PCR system (ABI PRISM 7700 Sequence Detection System; PE Applied Biosystems). To prepare standard RNA, PCR products were cloned into pBluescript vector and linearized at the T3 promoter site. Standard RNA was synthesized by using T7 RNA polymerase and purified by using Isogen (Wako Junyaku, Osaka, Japan) and deoxyribonuclease I (TaKaRa, Shiga, Japan). We detected HCV RNA in liver by using RTD-PCR as previously described.[38]

Statistical Analysis

All data are expressed as means ± SEM. Significance was tested by the Student *t* test and 1-way analysis of variance with Bonferroni's methods.

Results

Gene-Expression Profiling in Confluent or Serum-Starved Cells and the Activities of Hepatitis C Virus Internal Ribosomal Entry Site–Directed Translation

RCF-26 cell lines constitutively express dicistronic RNA transcripts containing sequences encoding the reporter proteins RL and FL separated by a functional HCV IRES (Figure 1). The activities of these proteins expressed in RCF-26 cells reflect cap-dependent and HCV IRES–directed translation, respectively. To rule out the possibility that FL activity from the second cistron reflected the nonspecific ribosomal scanning rather than HCV IRES–directed translation, we evaluated RL and FL activities in ΔRCF-9 cells in which the functional HCV IRES element had been deleted. The ratio of FL to RL (relative HCV IRES activity) in ΔRCF-9 was 2.5% of that in RCF-26, thus reflecting the specificity of HCV IRES activity in RCF-26 cells (Figure 2*B–D*).

To examine the relationship of the cellular proteins that vary in abundance and HCV IRES activities, RCF-26 cells and ΔRCF-9 cells were cultured in 15-cm dishes at confluence or under serum depletion for 48 hours, and changes in cellular gene expression and HCV IRES activities were evaluated. Under these conditions, the cellular DNA content increased at G_0/G_1 phase (49% to 74% in confluent cells and to 59% in serum-starved cells) and decreased at S phase (38% to 18% in confluent cells and to 35% in serum-starved cells) or G_2/M phase (14% to 8% in confluent cells and to 6% in serum-starved cells; Figure 2*A*). The degree of changes during the cell cycle was much greater in the confluent cells than in the serum-starved cells. The activities of HCV IRES–directed translation were reduced to 24% in confluent cells and to 22% in serum-starved cells compared with controls (Figure 2*C* and *D*), whereas the activities of cap-dependent cellular translation were essentially maintained (Figure 2*B*). Neither a significant difference in FL activity nor relative HCV IRES activity was found in ΔRCF-9 under these conditions (Figure 2*C* and *D*).

These results were not due to variations in the RNA stability of the RL and FL reporter genes. Northern blotting of mRNA transcribed from dicistronic constructs containing sequences encoding these 2 reporter proteins did not show either RNA degradation or splicing (data not shown). The relative expression ratio of mRNA of RL to FL determined by cDNA microarray did not change in either confluent or serum-starved cells (Figure 2*E*).

Gene-expression profiling changed in response to these conditions listed in Table 1. Serum proteins such as α_2-macroglobulin and albumin, as well as cell adhesion molecules such as cadherin, major histocompatibility complex, and fibronectin, were up-regulated by more than 1.8-fold. Albumin, a major serum protein that is specifically produced in the liver, was remarkably regulated in a cell-cycle dependent manner. However, cell-cycle and growth-related genes such as cyclin A, cyclin B, CDK1, cell division cell cycle 18, p53, hepatoma-

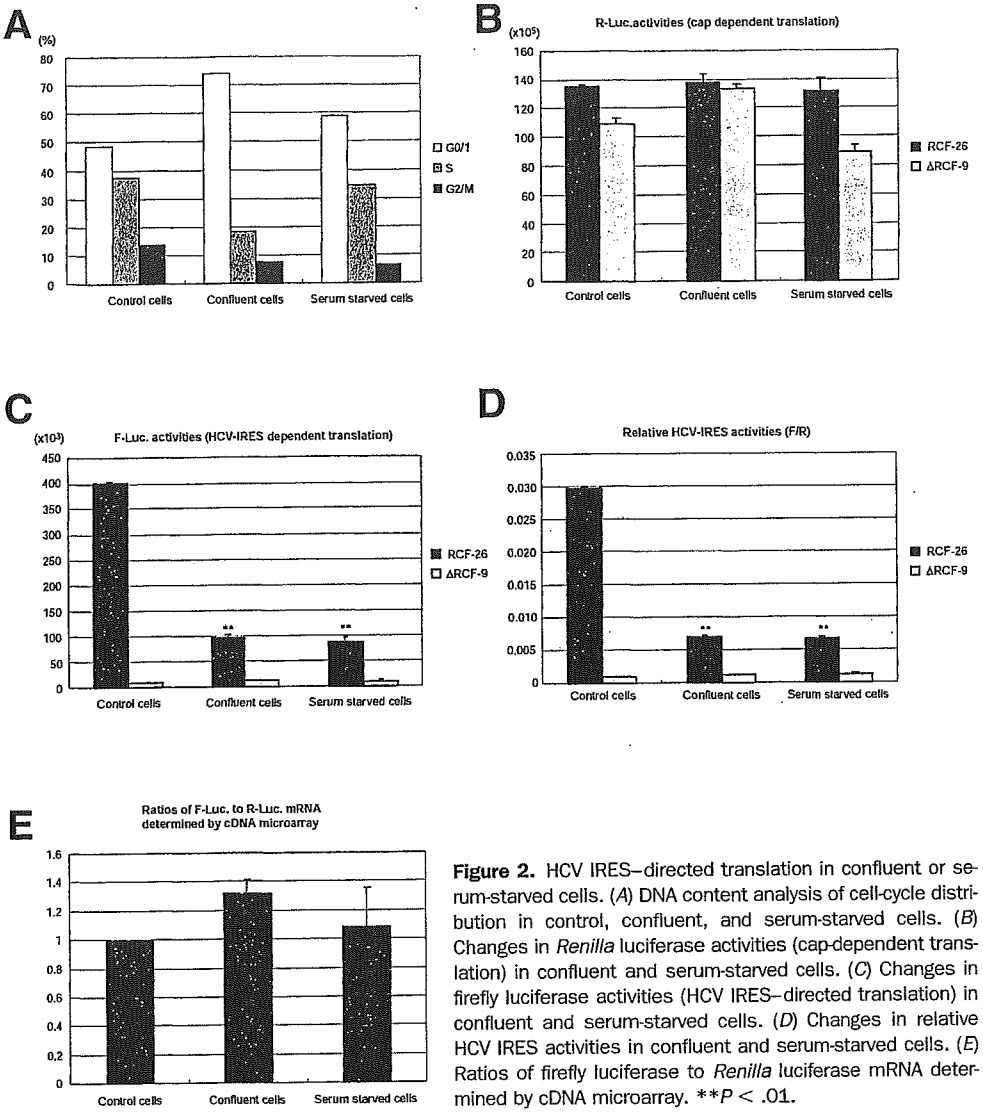

Figure 2. HCV IRES–directed translation in confluent or serum-starved cells. (*A*) DNA content analysis of cell-cycle distribution in control, confluent, and serum-starved cells. (*B*) Changes in *Renilla* luciferase activities (cap-dependent translation) in confluent and serum-starved cells. (*C*) Changes in firefly luciferase activities (HCV IRES–directed translation) in confluent and serum-starved cells. (*D*) Changes in relative HCV IRES activities in confluent and serum-starved cells. (*E*) Ratios of firefly luciferase to *Renilla* luciferase mRNA determined by cDNA microarray. $^{**}P < .01$.

derived growth factor, and nm23 were down-regulated, as were genes related to RNA polymerase, such as RNA polymerase II, subunit 5-mediating protein (RMP), La protein, and topoisomerase II. The La protein binds the stem loop IV structure in HCV IRES and stimulates HCV IRES–directed translation.[16,17] With regard to changes in the expression of canonical and noncanonical initiation factors (Table 2), La protein and PTB expression were repressed in both confluent and serum-starved cells. The expression of eIF3 (p170 and p116) was predominantly repressed in confluent cells, and the expression of eIF2γ was predominantly repressed in serum-starved cells. Conversely, the expression of ribosomal protein S9 and PABPC-1 was induced in confluent cells. The degree to which gene expression changed was more predominant in confluent cells than in serum-starved cells. This might reflect the greater degree of changes in the cell-cycle distribution of G_0/G_1 and S phases in confluent cells than in serum-starved cells (Figure 2*A*). The results of northern blots of La protein, PTB, and albumin expression coincided with these results (Figure 3). We evaluated changes in La protein and PTB expression by using RTD-PCR. The relative expression of La protein in confluent and serum-starved cells was 16% and 33% of control cells, respectively. The relative expression of PTB in confluent and serum-starved cells was 10% and 26% of control cells, respectively (data not shown). These data suggest that several canonical and noncanonical initiation factors, such as La protein, PTB, eIF3, and eIF2γ, are initiation factors responsible for regulating HCV IRES activity in a cell cycle–dependent manner.